JCTC Journal of Chemical Theory and Computation

ARTICLE

pubs.acs.org/JCTC

Effective Time-Independent Calculations of Vibrational Resonance Raman Spectra of Isolated and Solvated Molecules Including Duschinsky and Herzberg−Teller Effects

Fabrizio Santoro,*[,†] Chiara Cappelli,*[,†,‡] and Vincenzo Barone[†,§]

[†]CNR−Consiglio Nazionale delle Ricerche, Istituto di Chimica dei Composti Organo Metallici (ICCOM-CNR), UOS di Pisa, Area della Ricerca, via G. Moruzzi 1, I-56124 Pisa, Italy

[‡]Dipartimento di Chimica e Chimica Industriale, Università di Pisa, via Risorgimento, 35 I-56126 Pisa, Italy

[§]Scuola Normale Superiore, Piazza dei Cavalieri, 7 I-56126 Pisa, Italy

Supporting Information

ABSTRACT: We present a method of modeling vibrational resonance Raman scattering (RRS) spectra of isolated and solvated systems with the inclusion of Franck−Condon (FC) and Herzberg−Teller (HT) effects and a full account for possible differences between the harmonic potential energy surfaces of the initial and resonant electronic states. It describes fundamentals, overtones, and combination bands and computes the RRS spectrum as a two-dimensional function of the incident and scattered frequencies. The theoretical foundations of the method are described and the differences with other currently available methodologies are outlined. Applications to the phenoxyl radical in the gas phase and indolinedimethine−malononitrile (IDMN) in acetonitrile and cyclohexane solution are reported, as well as comparisons with available experimental data.

I. INTRODUCTION

Resonance Raman scattering (RRS) refers to Raman scattering at wavelengths close to an electronic excitation of the molecule[1] (see Figure 1 for a pictorial view). Because of this peculiarity, RRS is able to provide information on electronically excited state properties and structure,[2] which is an outcome that only rarely is obtained through other experimental techniques, and for which the formulation of modern quantum mechanical (QM) models has instead reached a well-recognized maturity.[3]

The sensitivity of experimental RRS has largely improved recently,[4] so it is becoming a very valuable technique for the study of the structure and dynamics of biosystems and materials. However, the calculation of RRS spectral parameters is far from being common in the literature; some aspects of such a subject still remain unexplored. Most of the RRS calculations reported until now are based on the so-called Transform Theory (TT)[5] or on the short-time dynamics (STD) approach.[6,7] TT is rooted in the Kramers−Kronig relationship between the polarizability and the absorption spectrum and, in its most common version, derives relative resonance Raman intensities from the differences in the equilibrium structures between the ground and the resonant excited states and a lineshape function Φ attainable from the absorption spectrum. The STD method originates from the pioneering work by Heller and co-workers, and it is based on a time-dependent redefinition of the energy-frame Kramers, Heisenberg, and Dirac (KHD) expression for the polarizability tensor,[8,9] in terms of the dynamics of a wave packet. Although this approach is quite general, most of its practical applications actually use the STD expressions, which are valid when only the STD of the system is reflected in the RRS spectra, and, therefore, are well-suited for preresonance regimes.[6,7] In this limit, relative RRS intensities are expressed in terms of the resonant-state energy gradient at the ground equilibrium geometry; therefore, they do not require explicit time-dependent calculations. Because of that, STD is also generally known as the "gradient method". The time-independent analysis of Warshel and Dauber allows one to bridge the TT and STD approaches in the harmonic limit,[10] where simple relations hold between excited-state gradients and equilibrium geometry displacements. Recently, a computationally different approach has been reported.[11] There, RRS is obtained from the geometrical derivatives of the frequency-dependent resonance polarizabilities, calculated by including a finite lifetime of the electronic excited states, using time-dependent density functional theory (TD-DFT). Such a method still relies on a short-time approximation and is similar to the simple excited-state gradient approximation method if only one electronic excited state is important.

Most of the previous methods for the calculation of RRS focus on the calculation of the so-called "Albrecht A^{VI} term",[1,12] which implies that Herzberg−Teller (HT) vibronic couplings are completely discarded, so that only Franck−Condon (FC)-type scattering is considered in the theoretical formalism. Also, it is assumed that only one electronic excited state is relevant in the process, and that the potential energy surfaces (PES) of the ground and excited state are harmonic. In addition, ground and excited state normal modes and their frequencies are assumed to

Received: January 24, 2011
Published: April 29, 2011

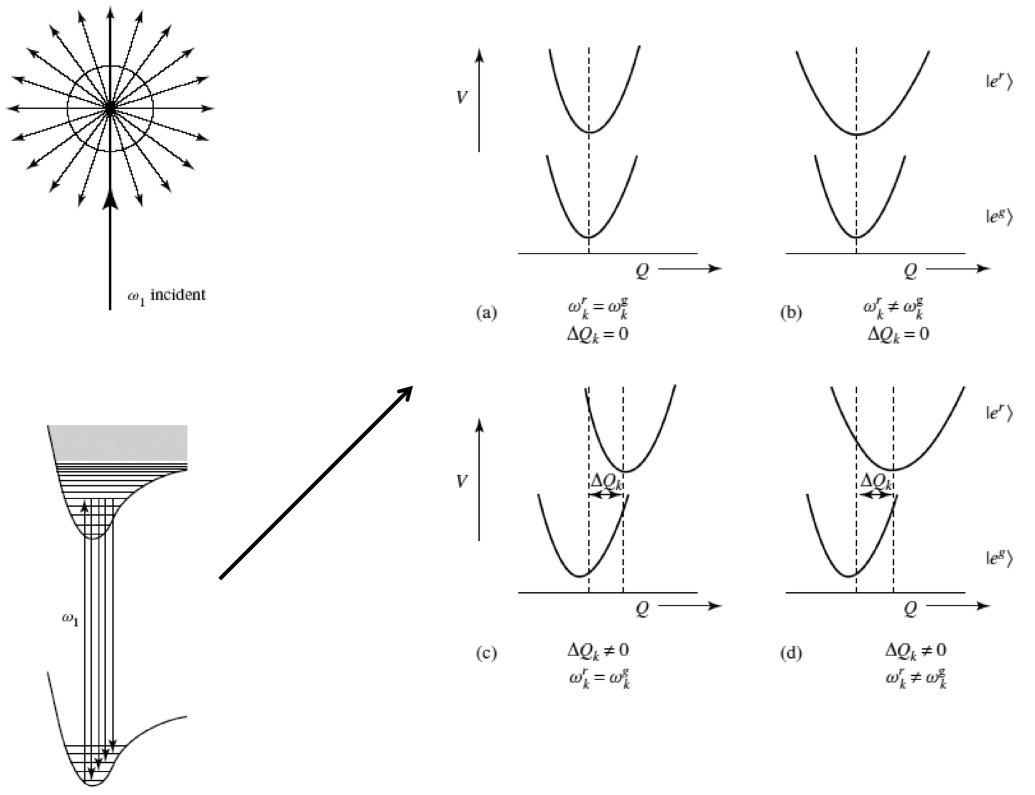

Figure 1. Pictorial view of the resonance Raman effect, along with a graphical representation of the various levels of treatment (a−d) of the ground (g) and excited (r) states potential energy surfaces: (a) $\omega_k^r = \omega_k^g$, $\Delta Q_k = 0$; (b) $\omega_k^r \neq \omega_k^g$, $\Delta Q_k = 0$; (c) $\omega_k^r = \omega_k^g$, $\Delta Q_k \neq 0$; and (d) $\omega_k^r \neq \omega_k^g$, $\Delta Q_k \neq 0$. Q stands for a normal coordinate, ΔQ is the displacement along that coordinate, and the ω terms are the vibrational frequencies associated with the Q values in the ground and excited states.

be identical ("independent mode, displaced harmonic oscillator model" (IMDHO)[13]) and excited- and ground-state normal coordinates are assumed to differ only in their equilibrium positions, so that Duschinsky rotations are not important. Finally, in most cases, only fundamental $0 \rightarrow 1$ transitions are considered, and the dependence on the incident frequency is not explicitly considered (although this is actually possible using both the TT theory[5] and the STD method[6,7]).

Within the above frameworks, several contributions have been presented in the literature, such as extensions to address anti-resonance contributions,[14] methods for the selective calculation of high-intensity modes,[15] computations of the lineshape function Φ entering in the TT expressions from sum over states approaches (and not from the experimental data),[16] corrections for the contributions of more than one resonant state,[17] extensions to resonance Raman optical activity,[18] as well as applications to interesting systems such as uracil,[19] pyrenes,[20] rhodamine,[21,22] julonidinemalononitrile chromophores,[23] and large ruthenium complexes.[24,25]

In this paper, we intend to present a general method rooted in the harmonic approximation that overcomes the approximations of the methods described above, using a time-independent sum-over-states (SOS) approach. We focus on vibrational RRS from the ground vibrational state $|\mathbf{0}^g\rangle$ (only Stokes bands), with the aim of describing both FC and HT effects (the so-called "Albrecht $B^{VI}-D^{VI}$ terms") and to fully account for any possible difference between the harmonic PES of the initial and resonant electronic states. In addition, the SOS approach, by explicitly computing the polarizability tensor, allows one to provide RRS spectra as a function of two frequency coordinates (two-dimensional (2D) RRS spectra)—the incident coordinate and scattered coordinate—and to account for interferential features arising from the contribution of more than one quasi-resonant electronic state. Recall that formal expressions to include Duschinsky and HT effects in the TT approach[26] and along the time-correlator formalism[27−29] have been derived in the past, and that the effect of HT[30] and Duschinsky mixings[31] has been addressed in simplified models for specific systems. However, a general tool for computing RRS spectra at the harmonic level is still lacking.

The basic ingredients to perform SOS RRS calculations, including Duschinsky and HT effects, are very similar to those required to compute absorption spectra. Namely, accurate formulas are needed to compute multidimensional FC integrals and, in large systems, effective prescreening methods must be able to select the relevant transitions among the very large number of possible quasi-resonant vibronic states (easily exceeding 10^{20}). While easily implemented recurrence formulas to compute FC integrals were derived a long time ago, through a generating function approach,[32−34] or a coherent state approach,[35,36] only recently effective selection schemes have been worked out (see ref 37 for a comprehensive review). They include specific partition in "levels" of the possible transitions[38] and selections through block factorization of the Duschinsky matrix,[39,40] or through analytical sum rules.[41]

We recently worked out a method based on partition of the possible transitions in classes C_n, depending on the number (n) of simultaneously excited modes in the final state, and a

prescreening method for high-order ($n > 2$) classes based on the analysis of C_1 and C_2 classes.[42] The method, which was originally worked out for FC 0 K one-photon absorption (OPA) and emission spectra, has been generalized to include temperature effects[43] and HT effects,[44] and to deal with one-photon circular dichroism (ECD)[45] and two-photon absorption and circular dichroism.[46] It has been recently implemented[47,48] for OPA and ECD in a optimized routine in the Gaussian 09 package.[49] Here, we present its further extension to 2D RRS spectra, exploiting the protocols developed for dealing with vibrationally excited initial states in finite temperature spectra[43] and including additional prescreening recipes on the final vibronic states of the ground electronic states, together with a generalization of analytical sum rules to check SOS calculation convergence.

It has been recognized that a very important role in RRS is played by the presence of a solvent,[4,21,50] because of the fact that the solute−solvent interactions can largely affect the electronic excited states, both by modifying their nature (the charge-transfer character is usually increased in polar solvents) and by inducing structural deformations, which can lead to very different relaxed excited states, with respect to their counterparts in the gas phase. In recent years, a method to couple TT and STD to continuum solvation models has been proposed.[51,52] In this paper, its further extension is reported, by also including the solvent effects on excited-state normal modes and transition dipoles, by exploiting the Polarizable Continuum Model (PCM).[53,54]

The paper is organized as follows. In the next section (section II), the theoretical background is summarized. After a brief section on computational details (section III), application of the methodologies to few selected systems in the gas phase or in solution is reported (section IV). Concluding remarks (in section V) end the presentation.

II. THEORETICAL FRAMEWORK

A. General Expression for Vibrational Resonance Raman Cross Section. We consider a monochromatic incident (I) radiation with angular frequency ω_I propagating in the direction of the unit vector $\mathbf{n}_0^I$, impinging on the sample, and we analyze the scattered radiation (s) of frequency ω_s in the propagation direction $\mathbf{n}_0^s$. The terms $\mathbf{n}_0^I$ and $\mathbf{n}_0^s$ define the so-called "scattering plane", and θ is the scattering angle ($\theta = \cos^{-1}(\mathbf{n}_0^I \cdot \mathbf{n}_0^s)$). Two possible polarizations for the incident and scattered light are, respectively, perpendicular ($\perp$) and parallel ($\parallel$) to the scattered plane. The scattered intensity at an angle of $\theta = 90°$ for any polarization ($\perp^s + \parallel^s$) for incident light with perpendicular polarization ($\perp^I$) is given as[1,55]

$$I\left(\frac{\pi}{2}; \perp^s + \parallel^s, \perp^I\right) = \frac{\omega_s^4 \mathscr{I}}{16\varepsilon_0^2 c_0^4 \pi^2} \frac{45a^2 + 7g^2 + 5d^2}{45} \quad (1)$$

where $\mathscr{I}$ is the incident field irradiance, c_0 the speed of light, and ε_0 the electric permittivity in a vacuum. The orientational average has been taken into account by considering freely rotating molecules. The a, g, and d terms are functions of the molecular polarizability tensor and, therefore, are dependent on ω_I and ω_s, as well as on molecular parameters; they are the so-called "mean polarizability", "symmetric anisotropy", and "antisymmetric anisotropy", respectively, and their explicit expressions are given below. Removing the dependence on $\mathscr{I}$, a differential cross section (with respect to a scattering solid angle Ω) is defined:

$$\sigma'(\omega_I, \omega_s) = \frac{\partial \sigma}{\partial \Omega} = \frac{I(\pi/2; \perp^s + \parallel^s, \perp^i)}{\mathscr{I}} \quad (2)$$

Note that an alternative definition of $\sigma'(\omega_I, \omega_s)$ is reported by some authors, not in terms of unit incident irradiance ($\mathscr{I}$), but per unit of incident photon flux ($\mathscr{I}/\hbar\omega_I$). In this case, the second differential cross section $\sigma''(\omega_I, \omega_s)$ (where $\sigma''(\omega_I, \omega_s) = \partial^2\sigma/\partial\Omega\partial\omega_s$), which is dependent on $\omega_s^3\omega_I$ rather than ω_s^4 (see eq 2), is reported.

We now introduce the polarizability tensor for a transition $|i\rangle \rightarrow |f\rangle$. Its $\rho\sigma$th element ($\rho, \sigma = x, y, z$) is

$$\alpha_{\rho\sigma}^{fi} = \frac{1}{\hbar}\sum_m \frac{\langle f|\mu_\rho|m\rangle\langle m|\mu_\sigma|i\rangle}{\omega_{mi} - \omega_I - i\gamma_m} + \frac{1}{\hbar}\sum_m \frac{\langle f|\mu_\rho|m\rangle\langle m|\mu_\sigma|i\rangle}{\omega_{mi} + \omega_I + i\gamma_m} \quad (3)$$

where μ_ρ is the ρ-Cartesian component of the electric dipole. The sum is taken over all possible intermediate states $|m\rangle$, $\omega_{mi} = \omega_m - \omega_i$; $\hbar\omega_i$ and $\hbar\omega_m$ are the energies of states $|i\rangle$ and $|m\rangle$, respectively; and, finally, γ_m is the lifetime of excited state $|m\rangle$. In the framework of the Born−Oppenheimer approximation (BO) and by considering, in eq 1, rotational states to be factorized out and summation over all possible orientations, we must address the vibronic states, which can be written as a product

$$|e_k; v_l^k\rangle = |e_k> \otimes |v_l^k\rangle$$

where $|e_k\rangle$ is the electronic state and $|v_l^k\rangle$ the associated vibrational state. The previously introduced a, g^2, and d^2 quantities are given as[1]

$$a = \frac{1}{3}(\alpha_{xx}^{fi} + \alpha_{yy}^{fi} + \alpha_{zz}^{fi}) \quad (4)$$

$$g^2 = \frac{1}{2}[|\alpha_{xx}^{fi} - \alpha_{yy}^{fi}|^2 + |\alpha_{xx}^{fi} - \alpha_{zz}^{fi}|^2 + |\alpha_{yy}^{fi} - \alpha_{zz}^{fi}|^2 + \frac{3}{2}\left(|\alpha_{xy}^{fi} + \alpha_{yx}^{fi}|^2 + |\alpha_{xz}^{fi} + \alpha_{zx}^{fi}|^2 + |\alpha_{yz}^{if} + \alpha_{zy}^{if}|^2\right)] \quad (5)$$

$$d^2 = \frac{3}{4}\left(|\alpha_{xy}^{fi} - \alpha_{yx}^{fi}|^2 + |\alpha_{xz}^{fi} - \alpha_{zx}^{fi}|^2 + |\alpha_{yz}^{if} - \alpha_{zy}^{if}|^2\right) \quad (6)$$

When the incident frequency is close to resonance with the transition energy ω_{mi}, the first resonant term in eq 3 dominates over the second off-resonant term, which can be safely neglected. Moreover, if both the initial and final states belong to the ground electronic state $|e_g\rangle$ (vibrational resonance Raman), by integrating over the electronic degrees of freedom, the following equation is obtained:

$$\alpha_{\rho\sigma}^{fi} = \sum_{k,m} \frac{\langle v_f^g|\mu_\rho^{gk}|v_m^k\rangle\langle v_m^k|\mu_\sigma^{kg}|v_i^g\rangle}{\omega_{km,gi} - \omega_I - i\gamma_k} \quad (7)$$

where $\mu_\beta^{gk} = \langle e_g|\mu_\beta|e_k\rangle$, $\omega_{km,gi} = \omega_{e_k} + \omega_{v_m^k} - (\omega_{e_g} + \omega_{v_i^g})$, and the lifetime γ_{km} of the intermediate states $|e_k; v_m^k\rangle$ is assumed to be independent from the vibrational state $|v_m^k\rangle$, so that it is possible to drop the m subscript out (γ_k). As shown by eq 2, the transition probability is dependent on the square of polarizability tensor elements. Therefore, when the exciting frequency is in near-resonance with the transitions to more than one excited electronic state $|e_k\rangle$, the sum in eq 7 must be carried out over all the

intermediate states, which can give rise to interferential features. Nonetheless, in this case, it also is possible to compute a polarizability tensor $\alpha_{\rho\sigma}^{gk}$ for each intermediate state $|e_k\rangle$ and obtain the total polarizability tensor by summing them up. Without any loss of generality, it is therefore possible, in the following, to refer to a single intermediate state $|e_k\rangle$, so that the summation over k will drop out.

B. The RR Cross Section in the Harmonic Approximation: Franck−Condon and Herzberg−Teller Terms. The discussion of the previous section has been carried out in very general terms. This section will focus the theory on the special cases where the PES of both the initial $|e^g\rangle$ and intermediate $|e^k\rangle$ electronic states can be treated within the harmonic approximation. In this case, vibrational states $|v_m^l\rangle$ of a given electronic state $|e_l\rangle$ are direct products of one-dimensional (1D) states $|m_j^l\rangle$ for each mode j, and $|v_m^k\rangle = |\mathbf{m}^k\rangle = |m_1^k\rangle\otimes|m_2^k\rangle...\otimes|m_N^k\rangle$, with N being the number of normal coordinates and m_j^k the quantum number of mode j.

According to Duschinsky,[56] the sets of mass-weighted normal coordinates $\mathbf{Q}^g$ and $\mathbf{Q}^k$ of electronic states $|e^g\rangle$ and $|e^k\rangle$ are related through a linear transformation:

$$\mathbf{Q}^g = \mathbf{J}\mathbf{Q}^k + \mathbf{K} \tag{8}$$

where $\mathbf{J}$ is the Duschinsky matrix and $\mathbf{K}$ is a column vector collecting the displacements between the equilibrium geometries of the two electronic PES.

The transition electric dipole $\vec{\mu}^{gk}$ generally is an unknown function of the normal coordinates. Its ρ Cartesian component can be written in terms of a Taylor expansion of the normal coordinates of the initial (ground) electronic state, $\mathbf{Q}^g$:

$$\mu_\rho^{gk} = \mu_\rho^{gk}(0) + \sum_j \mu_\rho^{gk}(j)Q_j^g + \sum_{j,l}\mu_\rho^{gk}(j,l)Q_j^gQ_l^g + ... \tag{9}$$

By restricting the expansion to the first order and substituting into eq 7, it follows that

$$\begin{aligned}\alpha_{\rho\sigma}^{fi} = {} & \frac{1}{\hbar}\sum_{\mathbf{m}}\frac{\langle\mathbf{n}^{f,g}|\mu_\rho^{gk}(0)|\mathbf{m}^k\rangle\langle\mathbf{m}^k|\mu_\sigma^{kg}(0)|\mathbf{n}^{i,g}\rangle}{\omega_{km,gi}-\omega_I-i\gamma_k} \\ & + \frac{1}{\hbar}\sum_{\mathbf{m}}\frac{\langle\mathbf{n}^{f,g}|\sum_l\mu_\rho^{gk}(l)Q_l^g|\mathbf{m}^k\rangle\langle\mathbf{m}^k|\mu_\sigma^{kg}(0)|\mathbf{n}^{i,g}\rangle}{\omega_{km,gi}-\omega_I-i\gamma_k} \\ & + \frac{1}{\hbar}\sum_{\mathbf{m}}\frac{\langle\mathbf{n}^{f,g}|\mu_\rho^{gk}(0)|\mathbf{m}^k\rangle\langle\mathbf{m}^k|\sum_j\mu_\sigma^{kg}(j)Q_j^g|\mathbf{n}^{i,g}\rangle}{\omega_{km,gi}-\omega_I-i\gamma_k} \\ & + \frac{1}{\hbar}\sum_{\mathbf{m}}\frac{\langle\mathbf{n}^{f,g}|\sum_l\mu_\rho^{gk}(l)Q_l^g|\mathbf{m}^k\rangle\langle\mathbf{m}^k|\sum_j\mu_\sigma^{kg}(j)Q_j^g|\mathbf{n}^{i,g}\rangle}{\omega_{km,gi}-\omega_I-i\gamma_k}\end{aligned} \tag{10}$$

The first term of eq 10 is the FC term, while the remaining terms arise from the HT borrowing mechanism of electronic transitions. By inspection of eq 10, it is apparent that the antisymmetric anisotropy d (eq 6) vanishes for pure FC transitions but is generally different from zero when the HT effect is considered. Adopting a second quantization,

$$\hat{Q}_l^g = \sqrt{\frac{\hbar}{2\omega_l}}\left(\hat{a}_l^{g,+} + \hat{a}_l^g\right)$$

we have

$$\begin{aligned}\hat{Q}_l^g|\mathbf{n}^{f,g}\rangle = {} & \sqrt{n_l^{f,g}+1}|\mathbf{n}^{f,g}+1_l\rangle \\ & + \sqrt{\mathbf{n}_l^{f,g}}|\mathbf{n}^{f,g}-1_l\rangle\end{aligned} \tag{11}$$

where $|\mathbf{n}^{f,g}+p_l\rangle$ is a vibrational state characterized by the same quantum numbers of $|\mathbf{n}^{f,g}\rangle$ for all modes except mode l, for which there are p_l additional quanta. Therefore, both FC and HT contributions can be computed if the generic FC overlap integrals $\langle\mathbf{n}^g|\mathbf{m}^k\rangle$ can be evaluated. Such integrals can be computed starting from the FC integrals between the ground vibrational states $\langle\mathbf{0}^g|\mathbf{0}^k\rangle$, according to the well-known recurrence formulas:[33,34,57]

$$\begin{aligned}\langle\mathbf{0}^g|\mathbf{m}^k\rangle = {} & \left(\frac{1}{2m_j^k}\right)^{1/2}A_j\langle\mathbf{0}^g|\mathbf{m}^k-1_j\rangle + \left(\frac{m_j^k-1}{m_j^k}\right)^{1/2}D_{jj}\langle\mathbf{0}^g|\mathbf{m}^k-2_j\rangle \\ & + \sum_{l,(l\neq j)}\left(\frac{m_l^k}{m_j^k}\right)^{1/2}D_{jl}\langle\mathbf{0}^g|\mathbf{m}^k-1_j-1_l\rangle\end{aligned} \tag{12}$$

$$\begin{aligned}\langle\mathbf{n}^g|\mathbf{m}^k\rangle = {} & \left(\frac{1}{2n_j}\right)^{1/2}B_j\langle\mathbf{n}^g-1_j|\mathbf{m}^k\rangle + \left(\frac{n_j^g-1}{n_j^g}\right)^{1/2}E_{jj}\langle\mathbf{n}^g-2_j|\mathbf{m}^k\rangle \\ & + \sum_{l,(l\neq j)}\left(\frac{n_l^g}{n_j^g}\right)^{1/2}E_{jl}\langle\mathbf{n}^g-1_j-1_l|\mathbf{m}^k\rangle \\ & + \sum_l\left(\frac{m_l^k}{n_j^g}\right)^{1/2}F_{jl}\langle\mathbf{n}^g-1_j|\mathbf{m}^k-1_l\rangle\end{aligned} \tag{13}$$

where

$$\begin{aligned}\mathbf{Y} &= \mathbf{J}^\dagger\mathbf{\Gamma}^g\mathbf{K} \\ \mathbf{X} &= \mathbf{J}^\dagger\mathbf{\Gamma}^g\mathbf{J} + \mathbf{\Gamma}^k \\ \mathbf{A} &= -2\mathbf{K}^\dagger\mathbf{\Gamma}^g\mathbf{X}^{-1}(\mathbf{\Gamma}^k)^{1/2} \\ \mathbf{D} &= 2(\mathbf{\Gamma}^k)^{1/2}\mathbf{X}^{-1}(\mathbf{\Gamma}^k)^{1/2} - \mathbf{I} \\ \mathbf{B} &= 2\mathbf{K}^\dagger(\mathbf{\Gamma}^g)^{1/2}(\mathbf{I} - (\mathbf{\Gamma}^g)^{1/2}\mathbf{J}\mathbf{X}^{-1}\mathbf{J}^\dagger(\mathbf{\Gamma}^g)^{1/2}) \\ \mathbf{E} &= 2(\mathbf{\Gamma}^g)^{1/2}\mathbf{J}\mathbf{X}^{-1}\mathbf{J}^\dagger(\mathbf{\Gamma}^g)^{1/2} - \mathbf{I} \\ \mathbf{F} &= 2(\mathbf{\Gamma}^g)^{1/2}\mathbf{J}\mathbf{X}^{-1}(\mathbf{\Gamma}^k)^{1/2}\end{aligned} \tag{14}$$

and $\mathbf{\Gamma}^g$ and $\mathbf{\Gamma}^k$ are diagonal matrices collecting the reduced frequencies $\omega_j^g/\hbar$ and $\omega_j^k/\hbar$, respectively, whereas $\mathbf{I}$ is the identity matrix. The FC integral between the ground states is[57]

$$\begin{aligned}\langle\mathbf{0}^g|\mathbf{0}^k\rangle = {} & (\det\mathbf{\Gamma}^g\det\mathbf{\Gamma}^k)^{1/4}\left(\frac{2^N\det\mathbf{J}}{\det\mathbf{X}}\right)^{1/2} \\ & \times\exp\left[-\frac{1}{2}\mathbf{K}^\dagger\mathbf{\Gamma}^g\mathbf{K} + \frac{1}{2}\mathbf{Y}^\dagger\mathbf{X}^{-1}\mathbf{Y}\right]\end{aligned} \tag{15}$$

Equations 10−13 are our working expressions. In the following, the treatment will be restricted to transitions from the ground vibrational state $|\mathbf{0}^g\rangle$, i.e., by definition to Stokes transitions $\omega_s < \omega_I$.

C. Comparison with Alternative Approaches. Limiting the discussion to time-independent methods only, as already reported in the Introduction, two main approaches have been

employed so far for the evaluation of RRS. The first one is based on the so-called "transform theory" (TT),[5] while the other is commonly known as the "short-time dynamics" (STD) method or the "gradient method".[6,7] For harmonic models, both approaches can be seen as particular cases of eq 10, and most of the reported calculations rely on the IMDHO model, where, as previously mentioned, the ground and excited PES share the same set of normal modes (i.e., for the Duschinsky matrix $\mathbf{J} = \mathbf{I}$) and there are no frequency changes (i.e., $\mathbf{\Gamma}^k = \mathbf{\Gamma}^g$).

In this case, the recurrence formulas in eqs 12 and 13 are drastically simplified, because the FC integrals can be written as products of one-dimensional (1D) integrals, and in eq 14, all the matrices except $\mathbf{F}$ vanish. Furthermore, $\mathbf{F} = \mathbf{I}$ and $\mathbf{A} = -\mathbf{B}$, with

$$A_j = -B_j = -K_j(\Gamma_j^g)^{1/2} = -\Delta_j \tag{16}$$

Note that $\Delta_j = K_j(\omega_j^g/\hbar)^{1/2}$ is the so-called "dimensionless displacement". Therefore, one simply obtains

$$\langle 0_j^g|m_j^k\rangle = -\frac{\Delta_j}{\sqrt{2m_j^k}}\langle 0_j^g|m_j^k - 1_j\rangle \tag{17}$$

$$\langle n_j^g|m_j^k\rangle = \frac{\Delta_j}{\sqrt{2n_j^g}}\langle n_j^g - 1_j|m_j^k\rangle + \sqrt{m_j^k/n_j^g}\langle n_j^g - 1_j|m_j^k - 1_j\rangle \tag{18}$$

In addition, the most popular and simplified approaches assume that HT contributions are negligible, and in eq 10, they only consider fundamental transitions $0_j \rightarrow 1_j$ for each mode j.

1. The Transform Theory. Let us start from a well-known relationship, which holds between the absorption cross section (Lorentzian broadening) and the polarizability tensor ($T = 0$ K is assumed):

$$\sigma_{\mathrm{abs}}(\omega_I) = C\omega_I \sum_{\mathbf{m}^k} |\langle \mathbf{0}^g|\mu^{g,k}|\mathbf{m}^k\rangle|^2 \frac{\gamma_k}{\pi[\omega_{kg} + \sum_j \omega_j^k m_j^k - \omega_I]^2 + \gamma_k^2}$$
$$= \frac{C}{\pi}\omega_I Im[\alpha_{xx}^{0,0} + \alpha_{xx}^{0,0} + \alpha_{xx}^{0,0}] \tag{19}$$

where C is a proportionality factor and ω_{kg} is the energy difference between the ground vibrational states associated to the two electronic states k and g. The explicit definition of such a factor has been previously reported in the literature[48] and is dependent on universal constants. By expressing all the parameters in atomic units, $\varepsilon(\omega_I)$ (given in dm^3 mol^{-1} cm^{-1}) is obtained (for a Lorentzian broadening). Let us further define a normalized cross section $\bar{\sigma}_{\mathrm{abs}}(\omega_I) = \sigma_{\mathrm{abs}}(\omega_I)/(\omega_I \int \sigma_{\mathrm{abs}}(\omega_I)/\omega_I\, \mathrm{d}\omega_I)$. By focusing on a FC case and considering a specific oscillator l, one can write

$$\bar{\sigma}_{\mathrm{abs}}(\omega_I) = \sum_{m_l} |\langle 0_l^g|m_l^k\rangle|^2 S(\omega_I - m_l^k\omega_l^k) \tag{20}$$

where, according to ref 19, we define

$$S(\omega_I - m_l^k\omega_l^k) = \sum_{m_j^k,\ \forall\, j\neq l} \frac{\Pi_{j\neq l}\langle|\mathbf{0}_l^g|\mathbf{m}_l^k|\rangle^2}{\pi[(\omega_{kg} + \sum_{j\neq l}\omega_j^k m_j^k) - (\omega_I - m_l^k\omega_l^k)]^2 + \gamma_k^2}$$

$$T(\omega_I - m_l^k\omega_l^k) = \sum_{m_j^k,\ \forall\, j\neq l} \frac{\Pi_{j\neq l}\gamma_k|\langle 0_j^g|m_j^k\rangle|^2[(\omega_{kg} + \sum_{j\neq l}\omega_j^k m_j^k) - (\omega_I - m_l^k\omega_l^k)]}{\pi[(\omega_{kg} + \sum_{j\neq l}\omega_j^k m_j^k) - (\omega_I - m_l^k\omega_l^k)]^2 + \gamma_k^2}$$

$$\Phi(\omega_I) = \sum_{m_l} |\langle 0_j^g|m_j^k\rangle|^2[T(\omega_I - m_l^k\omega_l^k) + iS(\omega_I - m_l^k\omega_l^k)] \tag{21}$$

Application of eq 18 gives

$$\langle 1_l^g|m_l^k\rangle = \frac{\Delta_l}{\sqrt{2}}\langle 0_l^g|m_l^k\rangle + \sqrt{m_l^k}\langle 0_l^g|m_l^k - 1_l\rangle$$

$$\langle m_l^k|0_l^g\rangle = -\frac{\Delta_l}{\sqrt{2m_l^k}}\langle 0_l^g|m_l^k - 1_l\rangle = \frac{\Delta_l^2}{2\sqrt{m_l^k(m_l^k - 1)}}\langle 0_l^g|m_l^k - 2_l\rangle$$

$$\langle 1_l^g|m_l^k\rangle\langle m_l^k|0_l^g\rangle = \frac{\Delta_l}{\sqrt{2}}[|\langle 0_l^g|m_l^k\rangle|^2 - |\langle 0_l^g|m_l^k - 1_l\rangle|^2]$$

$$\langle 2_l^g|m_l^k\rangle\langle m_l^k|0_l^g\rangle = \frac{\Delta_l^2}{2\sqrt{2}}[|\langle 0_l^g|m_l^k\rangle|^2 - 2|\langle 0_l^g|m_l^k - 1_l\rangle|^2 + |\langle 0_l^g|m_l^k - 2_l\rangle|^2]$$

$$\langle 1_j^g 1_l^g|m_j^k m_l^k\rangle\langle m_j^k m_l^k|0_j^g 0_l^g\rangle = \frac{\Delta_j\Delta_l}{2}[|\langle 0_l^g|m_l^k\rangle|^2 - |\langle 0_l^g|m_l^k - 1_l\rangle|^2] \times [|\langle 0_j^g|m_j^k\rangle|^2 - |\langle 0_j^g|m_j^k - 1_j\rangle|^2] \tag{22}$$

Such expressions are equivalent to those given by Neugebauer and Hess[19] in the case of $|0_l^g\rangle \rightarrow |1_l^g\rangle$ fundamental transitions and also extend them to the treatment of overtones $|0_l^g\rangle \rightarrow |2_l^g\rangle$ and combination bands $|0_j^g 0_l^g\rangle \rightarrow |1_j^g 1_l^g\rangle$. By further following Neugebauer and Hess,[19] one finally gets the following, for fundamentals:

$$\alpha_{\rho\sigma}^{0_l \rightarrow 1_l} = \mu_\rho^{gk}(0)\mu_\sigma^{gk}(0)\frac{\Delta_l}{\sqrt{2}}[\Phi(\omega_I) - \Phi(\omega_I - \omega_l)] \tag{23}$$

where $\Phi(\omega_I)$ is related to the normalized spectrum $\bar{\sigma}_{\mathrm{abs}}(\omega_I)$ through the following equation ($\mathscr{P}$ indicates the Cauchy principal-value integral):

$$\Phi(\omega_I) = i\pi\bar{\sigma}_{\mathrm{abs}}(\omega_I) + \mathscr{P}\int \mathrm{d}\omega \frac{\bar{\sigma}_{\mathrm{abs}}(\omega)}{(\omega - \omega_I)} \tag{24}$$

For the first overtone band, one similarly obtains

$$\alpha_{\rho\sigma}^{0_l \rightarrow 2_l} = \mu_\rho^{gk}(0)\mu_\sigma^{gk}(0)\frac{\Delta_l^2}{2\sqrt{2}}[\Phi(\omega_I) - 2\Phi(\omega_I - \omega_l) + \Phi(\omega_I - 2\omega_l)] \tag{25}$$

and, for the two-mode combination bands,

$$\alpha_{\rho\sigma}^{0_j 0_l \rightarrow 1_j 1_l} = \mu_\rho^{gk}(0)\mu_\sigma^{gk}(0)\frac{\Delta_j\Delta_l}{2} \times [\Phi(\omega_I) - \Phi(\omega_I - \omega_j) - \Phi(\omega_I - \omega_l) + \Phi(\omega_I - \omega_j - \omega_l)] \tag{26}$$

Note that eqs 23 and 25 hold whenever mode l is not mixed (i.e., $J_{ll} = 1$) and its frequency is unchanged in the two electronic states ($\Gamma_{ll}^g = \Gamma_{ll}^k$), and, therefore, also when Duschinsky mixing and frequency

changes take place for other modes (i.e., $\mathbf{J} \neq \mathbf{I}$ and/or $\mathbf{\Gamma}^g \neq \mathbf{\Gamma}^k$). The same also holds for eq 26 if both modes j and l fulfill these requirements. Therefore, eqs 23−26 can be utilized to estimate the intensities *a priori* for the modes that almost meet the conditions reported above. For instance, when Δ_l (and Δ_j) are small (i.e., $\ll 1$), fundamental transitions are expected to be the strongest ones.

2. The Gradient Approximation. Let us consider only FC terms in the polarizability tensor and only the fundamental transitions $0_j \rightarrow 1_j$ for each mode j. If $\Delta_j \ll 1$, as already noticed by Long[1] and by Warshel and Dauber,[10] it follows that $\langle 0_j^g | 0_j^k \rangle \approx \langle 1_j^g | 1_j^k \rangle \approx 1$ and $\langle 0_j^g | 1_j^k \rangle = -\langle 1_j^g | 0_j^k \rangle = -\Delta_j/\sqrt{2}$, while all the other integrals are zero. By neglecting all the terms beyond the first order in the displacements Δ_l, the polarizability tensor simply becomes

$$\alpha_{\rho\sigma}^{0_j \rightarrow 1_j} = \mu_\rho^{gk}(0)\mu_\sigma^{kg}(0)\left[\frac{\langle 0_j^g | 0_j^k\rangle\langle 0_j^k | 1_j^g\rangle}{\omega_{kg} - \omega_I - i\gamma_k} + \frac{\langle 0_j^g | 1_j^k\rangle\langle 1_j^k | 1_j^g\rangle}{\omega_{kg} + \omega_j - \omega_I - i\gamma_k}\right] \tag{27}$$

$$\alpha_{\rho\sigma}^{0_j \rightarrow 1_j} = \mu_\rho^{gk}(0)\mu_\sigma^{kg}(0)\frac{\omega_j\Delta_j}{\sqrt{2}(\omega_{kg} - \omega_I - i\gamma_k)(\omega_{kg} + \omega_j - \omega_I - i\gamma_k)} \tag{28}$$

where ω_{kg} is the electronic adiabatic energy difference. When $\omega_{kg} - \omega_I \gg \omega_j$, the denominator of last equation can be considered constant for different ω_j; therefore, the approximate relationships hold for the polarizability tensor component $\alpha_{\rho\sigma}^{0_j \rightarrow 1_j} \propto \Delta_j\omega_j$, and for the differential cross section $\sigma'^{0_j \rightarrow 1_j} \propto (\Delta_j\omega_j)^2$. Note that, in the limit of validity of the IMDHO model, Δ_j can be obtained avoiding geometry optimization of the excited state, by simply computing the derivative of the excited-state energy, with respect to the normal coordinate Q_j at the ground equilibrium geometry (the so-called "vertical gradient"):

$$\left(\frac{\partial E^k}{\partial Q_j}\right)_0 = E_j^k = -\omega_j^2 K_j = -\frac{\omega_j^{3/2}\Delta_j}{\hbar^{1/2}} \tag{29}$$

Therefore, it is possible to write that the ratio between the RRS intensities of the two modes j and l is

$$\frac{I_j^{0 \rightarrow 1}}{I_l^{0 \rightarrow 1}} = \left(\frac{E_j^k}{E_l^k}\right)^2\frac{\omega_l}{\omega_j} = \frac{\omega_j^2\Delta_j^2}{\omega_l^2\Delta_l^2} \tag{30}$$

To complete this section, it is worth recalling that, in a series of seminal papers,[6,7] Heller and co-workers showed, using a time-dependent approach, that, under preresonance conditions, when only the very short time dynamics on the excited state is to be considered, the first equality of eq 30 is still fulfilled; also, in case the IMDHO model is not valid and the second equality of eq 30 does not hold. In true resonance cases, even when the harmonic approximation is valid, eq 30 does not hold and Duschinsky mixing and frequency changes must be considered; this can be done via direct application of eq 10, thus also allowing for a detailed analysis of these effects.

III. COMPUTATIONAL METHOD: A DOUBLE-LAYER SELECTION SCHEME

As already stated in the Introduction, our aim is to focus on vibrational RR transitions from the ground vibrational state $|\mathbf{0}^g\rangle$ (only Stokes bands), to describe both Franck−Condon (FC) and Herzberg−Teller (HT) effects, and to fully account for any possible difference between the harmonic PES of the initial and intermediate electronic states. Our working expressions for intensity are eqs 1−6, while the polarizability tensor for each intermediate electronic state $|e^k\rangle$ is computed according to eq 10.

As reported above, the necessary integrals on the vibrational coordinates can be computed according to recurrence formulas (see eqs 12 and 13). However, such a treatment can be very cumbersome from the computational point of view, for two main reasons. The first one is that the explicit calculation of the polarizability tensor, in terms of a brute-force SOS expression, is generally unfeasible, because the number of vibrational states of the intermediate electronic state in a sizable molecule is huge (can easily exceed 10^{20}). Note that, in fact, if one wants to compute the RRS spectra as a function of the excitation frequency, all the vibronic transitions relevant for the absorption spectrum of the resonant state must be taken into account. The second reason is that the number of possible final vibrational states (i.e., those belonging to the ground electronic state) also is extremely large. Thus, in order to make the calculation feasible, it is necessary to work out effective prescreening techniques that are able to select only the relevant contributions *a priori*. Here, we will propose a way to overcome such difficulties using a two-layer strategy, by keeping in mind the fact that, although a too-strict selection of the final states may result in the absence of some bands in the simulated RR spectrum, an incomplete inclusion of the intermediate states may lead to inaccuracies in the predicted bands, which cannot easily be controlled.

A. Selection of the Intermediate States. Upon inspection of eq 10, it can be realized that, by resorting to an SOS time-independent perspective, the computation of the polarizability tensor for a given final state $|\mathbf{f}^g\rangle$ (the initial state is always the ground state $|\mathbf{0}^g\rangle$) is equivalent to the computation of two absorption spectra (possibly including HT effects) for the electronic transition $|e^g\rangle \rightarrow |e^k\rangle$. The first one arises from the ground vibrational state $|\mathbf{0}^g\rangle$ (for $T = 0$ K), and the second arises from a selected hot-vibrational state $|\mathbf{f}^g\rangle$. If more than one intermediate electronic state $|e^k\rangle$ is to be considered, the calculation should be repeated for each state and the polarizability tensors summarized before computing the square contributions to eq 2. An effective method to compute absorption spectra including Duschinsky and HT effects both for $T = 0$ K and finite temperature spectra has been proposed previously by some of us.[42−44] It is intuitive that the machinery that permits the computation of spectra at finite temperature also allows, in a straightforward manner, the computation of the spectrum from a single hot state $|\mathbf{f}^g\rangle$.

In brief, our method is based on a partition of the manifold of vibrational states $|\mathbf{m}^k\rangle$ of the resonant state $|e^k\rangle$ (and of the corresponding transitions) in different classes C_n, each depending on the number n of oscillators, whose quantum number is different from zero. For instance, $\langle \mathbf{n}^g | 3, 0, ...\rangle$ is a C_1 transition, and $\langle \mathbf{n}^g | 0, 3, 0, 5, 4, 0, ...\rangle$ is a C_3 transition. For each C_n, a maximum-allowed excitation vector $\mathbf{W}_n^{\max}(\mathbf{n}^g)$ is defined, so that all the integrals $\langle \mathbf{n}^g | \mathbf{m}^k\rangle$ to states $|\mathbf{m}^k\rangle$ with larger quantum numbers can be considered as negligible. In the general case of a finite-temperature spectrum with HT effects, the determination of $\mathbf{W}_n^{\max}(\mathbf{n}^g)$ is based on the analysis of the C_1 and C_2 FC transitions (which involve a low computational cost), both from the ground and from the excited initial states (in our case, $|\mathbf{0}^g\rangle$ and $|\mathbf{f}^g\rangle$), with the addition of the HT contribution to the C_1 class.[44] For further details, the interested reader is directed to the cited references.

Because of the recursive nature of the formulas in eqs 12 and 13, the calculation of the spectrum from the $|\mathbf{f}^g\rangle$ state automatically provides all the data that are required for the computation of the spectrum from any state $|\mathbf{f}'^g\rangle$, as far as $f'^g_j \leq f^g_j$ for $\forall j$. In the cited references, such a feature was exploited in the computation of the finite temperature spectra, by grouping the Boltzmann-populated initial states into "mother states", which are used for the calculation of the spectra for all the initial states that share the same set of initially excited normal modes.

Here, we will exploit the recursive properties of the method by performing separate calculations for the overtones of each normal mode j, up to a given quantum f_j (i.e., by adopting the initial state $|\mathbf{f}^g\rangle = |\mathbf{0}^g + f^g_j\rangle$), and also by collecting, in this way, the information for lower overtones and fundamentals. In an analogous way, for combination bands, a separate calculation for each couple (j, l) up to quanta f_j and f_l can be performed (i.e., selecting the initial state $|\mathbf{f}^g\rangle = |\mathbf{0}^g + f^g_j + f^g_l\rangle$), to gather the information needed for any less-excited combination band of the same couple j and l.

B. Selection of the Final Vibrational States of the Ground Electronic State. In principle, the number of the possible final states of the ground electronic states populated upon RRS is not limited by any strict selection rule. However, experimental RRS spectra are usually measured in a rather narrow energy window, only encompassing fundamentals and low-excited overtones and combination bands. Concerning theoretical simulations, most of those reported in the literature so far consider only fundamental bands.

Here, we will focus on fundamentals, overtones, and combination bands of two modes, and we will adopt simple selection schemes, based on the analysis of the TT predictions within the IMDHO model. In practice, we exclude from the calculation all of the modes that are essentially not mixed by Duschinsky couplings and that show displacements and frequency changes that are below a given threshold. For all the other modes, fundamentals and overtones are computed up to the same maximum quantum number. The analysis of the fundamentals and overtones is used to guess the most important combination bands of two modes, by sorting the modes in decreasing order of RRS intensities for fundamentals and by further selecting the first N_r modes for which combination bands are actually computed, that, in order to keep the number of initial states for combination bands $N_r^*(N_r - 1)/2$ below a given maximum number. This very simple selection is based on the observation that, in the limit of validity of the IMDHO model, according to TT predictions (see eqs 23−26), fundamental intensities are dependent on dimensionless displacements and $(1 + 1)$ combination bands on their product; therefore, the combination bands of two modes showing negligible fundamentals is expected to be negligible (unless very strong Duschinsky mixings take place). More-refined selections are obviously possible, but the investigation of such a matter will be postponed to future work.

C. Analytical Sums and Convergence Checks. It is worthy to note that, when the transition is off-resonant $\omega_I \ll \omega_{km,gi}$, the denominator in eq 10 can be considered constant and equal to $\omega_{kg} - \omega_I$ for each intermediate electronic state $|e_k\rangle$. Therefore, it is possible to sum over the vibrational $\mathbf{m}^k$ states and, by exploiting the closure relationship $\sum_{v^k_m} |v^k_m\rangle\langle v^k_m| = 1$, one can easily prove that the FC term vanishes. In those particular cases, the dominant terms in the polarizability tensor that determine the transition intensity are the HT terms (i.e., those depending linearly on the normal coordinates $\mathbf{Q}^g$). Obviously, when $\omega_I \ll \omega_{km,gi}$, the second term in the right-hand side (rhs) of eq 3 cannot be considered negligible in comparison with the first term, however, its FC contribution also vanishes, thus making the FC contribution to Raman scattering null. In the resonant case, both FC and higher-order terms may contribute to the polarizability tensor and FC terms are expected to dominate for strongly allowed transitions, i.e., when $|\vec{\mu}^{gk}(0)| \gg |\sum_l \vec{\mu}^{gk}(l)\Delta Q_l|$, where now $\vec{\mu}$ is the vector (μ_x, μ_y, μ_z) and ΔQ_I represents the displacements of the equilibrium structures caused by the electronic transition along mode I.

To compute the RRS intensities through the SOS expression in eq 10, the number of intermediate vibronic states to be considered is, in principle, infinite, and clearly the sum must be truncated. Moreover, Duschinsky effects prevent easy routes to accelerate the calculations. Therefore, it is useful to work out analytical sum rules in order to check the convergence of the results. As already discussed, the calculation of RRS intensities can be reduced to the calculation of two absorption spectra, and, therefore, the same analytical sums that have been derived in previous papers[44] also can be useful for RRS.

In addition, the off-resonant limit of the polarizability tensor provides a suitable route to obtain new and specific sum rules for RRS. In fact, by skipping the denominators in eq 10, we obtain

$$\begin{aligned}\bar{\alpha}^{f0}_{\rho\sigma} = &\sum_{\mathbf{m}} \langle \mathbf{0}^g|\mu^{gk}_\rho(0)|\mathbf{m}^k\rangle\langle\mathbf{m}^k|\mu^{kg}_\sigma(0)|\mathbf{f}^g\rangle \\ &+ \sum_{\mathbf{m}} \langle \mathbf{0}^g|\sum_l \mu^{gk}_\rho(l)Q^g_l|\mathbf{m}^k\rangle\langle\mathbf{m}^k|\mu^{kg}_\sigma(0)|\mathbf{f}^g\rangle \\ &+ \sum_{\mathbf{m}} \langle \mathbf{0}^g|\mu^{gk}_\rho(0)|\mathbf{m}^k\rangle\langle\mathbf{m}^k|\sum_j \mu^{kg}_\sigma(j)Q^g_j|\mathbf{f}^g\rangle \\ &+ \sum_{\mathbf{m}} \langle \mathbf{0}^g|\sum_l \mu^{gk}_\rho(l)Q^g_l|\mathbf{m}^k\rangle\langle\mathbf{m}^k|\sum_j \mu^{kg}_\sigma(j)Q^g_j|\mathbf{f}^g\rangle \end{aligned} \quad (31)$$

and by summing over the intermediate vibrational states, we get

$$\begin{aligned}\bar{\alpha}^{f0}_{\rho\sigma} = &\mu^{gk}_\rho(0)\mu^{kg}_\sigma(0)\langle\mathbf{0}^g|\mathbf{f}^g\rangle + \mu^{kg}_\sigma(0)\sum_l \mu^{gk}_\rho(l)\langle\mathbf{0}^g|Q^g_l|\mathbf{f}^g\rangle \\ &+\mu^{gk}_\rho(0)\sum_j \mu^{kg}_\sigma(j)\langle\mathbf{0}^g|Q^g_j|\mathbf{f}^g\rangle \\ &+ \sum_{l,j} \mu^{gk}_\rho(l)\mu^{kg}_\sigma\langle\mathbf{0}^g|Q^g_l Q^g_j|\mathbf{f}^g\rangle \end{aligned} \quad (32)$$

The above integrals are easily evaluated (for example, switching to a second quantization), giving

$$\bar{\alpha}^{f0}_{\rho\sigma} = \left\{ \begin{array}{ll} \mu^{gk}_\rho(0)\mu^{kg}_\sigma(0) + \sum_l \mu^{kg}_\rho(l)\mu^{kg}_\sigma(l)\dfrac{\hbar}{2\omega^g_l} & \text{if } |\mathbf{f}^g\rangle \equiv |\mathbf{0}^g\rangle \\ (\mu^{gk}_\rho(0)\mu^{kg}_\sigma(l) + \mu^{gk}_\rho(l)\mu^{kg}_\sigma(0))\sqrt{\dfrac{\hbar}{2\omega^g_l}} & \text{if } |\mathbf{f}^g\rangle \equiv |\mathbf{0}^g + 1_l\rangle \\ (\mu^{gk}_\rho(l)\mu^{kg}_\sigma(j) + \mu^{gk}_\rho(j)\mu^{kg}_\sigma(l))\dfrac{\hbar}{2\sqrt{\omega^g_l\omega^g_j}} & \text{if } |\mathbf{f}^g\rangle \equiv |\mathbf{0}^g + 1_l + 1_j\rangle \\ \mu^{gk}_\rho(l)\mu^{kg}_\sigma(l)\dfrac{\sqrt{2}\hbar}{2\omega^g_l} & \text{if } |\mathbf{f}^g\rangle \equiv |\mathbf{0}^g + 2_l\rangle \\ 0 & \text{for all other final states} \end{array} \right\} \quad (33)$$

When performing the SOS calculation of the RRS intensity for a given final state $|\mathbf{f}^g\rangle$, it is thus possible to compute numerical quantities $\bar{\alpha}^{num}_{\rho\sigma}$, analogous to the analytical $\bar{\alpha}_{\rho\sigma}$ ones, by adding all the contributions for each different intermediate state

considered, $|\mathbf{m}^k\rangle$. Comparison of numerical and analytical sums permits one to check the convergence of the calculations.

IV. APPLICATIONS

Here, the methodology described in the previous sections to evaluate RRS is applied to selected systems, i.e., the phenoxyl radical in the gas phase, and indolinedimethine−malononitrile (IDMN) in an acetonitrile and cyclohexane solution. These two cases were chosen because of the availability of experimental data in the literature that allow for a critical comparison of the accuracy of our computations and a detailed analysis of performance of the various levels of approximation. Although our approach, in principle, is applicable to any electronic structure method that can locate equilibrium structures of ground and excited states and their Hessian matrices, in the following, we will refer to TD-DFT calculations for mere computational convenience.

In parallel to the presentation of RRS spectra, we also report and discuss absorption spectra of the various systems, in order to evaluate the overall performance of TD-DFT in reproducing excitation energies, vibronic band profiles, and states hierarchy, and to identify the electronic states that are in resonance with a certain excitation frequency exploited in the RRS spectra.

A necessary starting point for the simulation is to locate the equilibrium geometry of the ground electronic state and to perform a normal-mode analysis in order to establish a harmonic model of the ground PES (V_g). In addition, both RRS and absorption spectra calculation rely on the specific model of the excited (resonant) state PES (V_k). Vertical (V) and adiabatic (A) approaches can be exploited, depending whether the excited PES is expanded in a Taylor series of the nuclear coordinates around its own equilibrium geometry ("A" approach) or around the ground-state geometry ("V" approach). Moreover, when only constant and linear terms are retained in the Taylor expansion of the difference $V_k - V_g$, the model implicitly assumes that normal modes and frequencies are the same in the two states and only the equilibrium geometries are displaced (IMDHO model). In this framework, if displacements are obtained from the excited-state gradient at the ground-state geometry, we have the so-called "Vertical Gradient" (VG) model; alternatively, if they are directly obtained as the difference in the equilibrium geometries, a different model—which we call the "Adiabatic Shift" (AS) model—is obtained.

In order to account not only for displacements, but also for frequency changes and Duschinsky mixings, it is necessary to compute the excited-state Hessian, thus obtaining the Vertical Hessian (VH) or Adiabatic Hessian (AH) models, depending on the reference geometry. The model for the computation is complete if the approximation for the transition electric dipole is specified, namely, if only the constant (FC) terms, the linear (HT) terms, or both (FC + HT) terms are considered in the expansion (see eq 9).

In the following, we will compare the results obtained from SOS expressions for absorption and RRS spectra (see eqs 20 and 10), according to FC|AS, FC|AH, and (FC + HT)|AH models (for the sake of brevity, "FC + HT" will be abbreviated hereafter as HT; this generates no confusion, since we never show the pure HT contributions alone). In the case of RRS spectra, in order to highlight the differences between our method and the ones mostly exploited in the literature so far, we will also report the FC results obtained according to the gradient (VG) approximation (TT spectra are usually computed by skipping the Φ factor and, therefore, are assimilable to VG results).

All the electronic calculations that will be reported were performed by exploiting the Gaussian09[49] package. Vibronic FC[42] and HT[44] calculations were done using a modified version of the *FCclasses* code;[58] in the latter, the convergence of the results is ruled by a user-defined parameter $N^{\max}$, which limits the number of possible transitions to be computed for each excitation class n. Increasing $N^{\max}$ results in a better convergence (hence, better quality of the results) but also increases the computational burden; therefore, a compromise must be chosen. Convergence of absorption and RRS was checked according to the analytical sums given in eq 33, as well as by direct comparison of the spectra obtained with different choices of $N^{\max}$. RRS spectra appeared to converge much faster than the analytical sums, which is a favorable feature that was already observed for absorption spectra.[42]

When required, solvent effects were taken into account using the PCM,[53,54] by setting cavity parameters as well as the proper static and optical dielectric constant values according to Gaussian09[49] default values.

A. The Phenoxyl Radical in the Gas Phase. *1. Absorption Spectrum.* In Figure 2, calculated excitation energies from the doublet $^2B_1$ ground state D_0 to the first five OPA allowed electronic excited states of the phenoxyl radical in the gas phase are reported (C_{2v} symmetry) . Following ref 40, the uB3LYP/TZVP level was selected, among others. As can be seen from the results reported in the figure, such a level performs in a manner pretty similar to that of the uB3LYP/cc-PVTZ level (which was already proposed for this molecule by Radziszewski et al.[59]) and to the 6-31+G(d,p), 6-31++G(d,p) and 6-311+G(d,p) basis sets. The level of reproduction of the experimental excitation energies is almost independent of the choice of the basis set, and it is pretty good overall, with the maximum deviation being of the order of 0.4 eV. Because of this fact, the following discussion will be limited to the uB3LYP/TZVP results.

Figure 3 sketches the calculated absorption spectrum of the phenoxyl radical, and the FC|AS, FC|AH, and HT|AH approaches are compared by focusing on the transitions to states D_2 ($^2B_2$) and D_3 ($^2A_1$), since the transition to D_1 is extremely weak. In order to simulate inhomogeneous broadening, stick spectra have been convoluted with a Gaussian lineshape, whose width is indicated in the figure caption. As is evident upon inspection of the calculated spectra, the role of HT is quite marginal for the D_2 spectrum (panel a), whereas a more substantial effect is noticed on relative intensities of the various vibronic peaks of the D_3 transition (panel b). One dominant progression can be singled out in the $D_0 \rightarrow D_2$ absorption spectrum, along mode $\nu_6^{(2)}$ (the number in parentheses specifies the electronic state, $0 \equiv g$), whose frequency is 522 cm^{-1}; this mode is projected for more than 99% on ground-state mode $\nu_5^{(0)}$, and it corresponds to a 1,4 elongation of the phenyl ring; secondary progressions involve three modes in the 1550−1600 cm^{-1} range. The main vibrational progressions in the D_3 spectrum are due to $\nu_{23}^{(3)}$ (1499 cm^{-1}), $\nu_{19}^{(3)}$ (1278 cm^{-1}) and $\nu_{14}^{(3)}$ (927 cm^{-1}). Notice that $\nu_{23}^{(3)}$ and $\nu_{19}^{(3)}$ show the largest derivatives of $\vec{\mu}^{03}$; however, interestingly, HT leads to a decrease of their vibronic intensities (as they become lower than the fundamental of $\nu_{14}^{(3)}$), because of partial destructive interference. The approximations of the AS model, with respect to the AH model, manifest themselves in a general blueshift of the spectrum, because of neglect of the zero-point energy differences in the ground and resonant electronic states, and in some redistribution

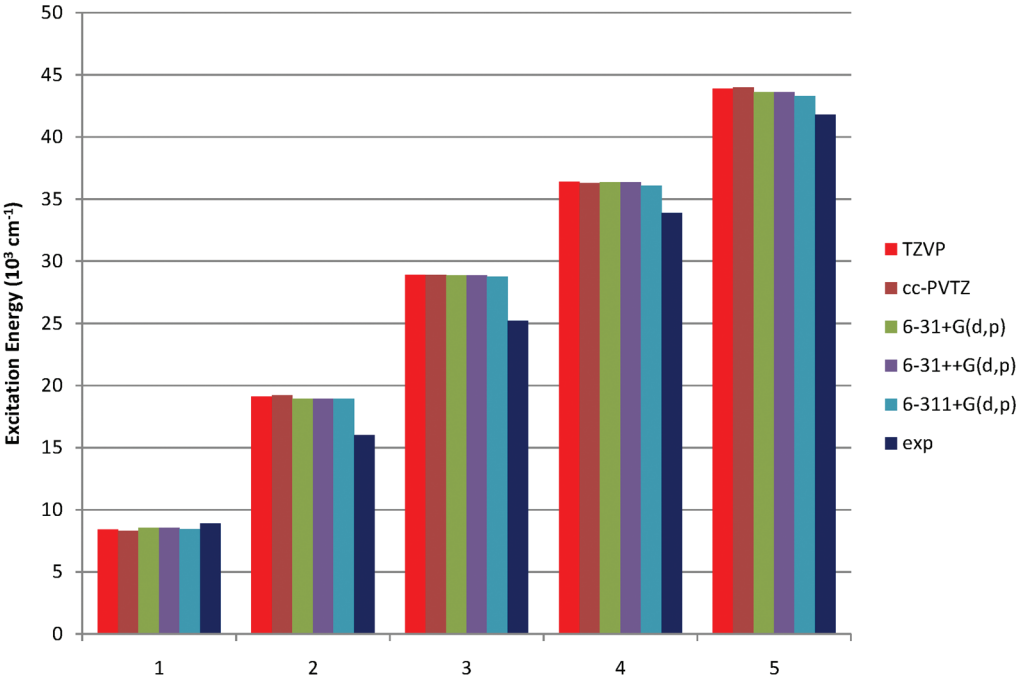

Figure 2. Calculated excitation energies of the first five OPA allowed electronic states of phenoxyl radical in the gas phase, as obtained using the B3LYP functional and different basis sets. Symmetry assignments are done according to the orientation reported in Figure 3 and are as follows: (1) $^2A_2$, (2) $^2B_2$, (3) $^2A_1$, (4) $^2B_2$, and (5) $^2A_1$. For comparison, experimental excitation energies taken from ref 59 are also reported.

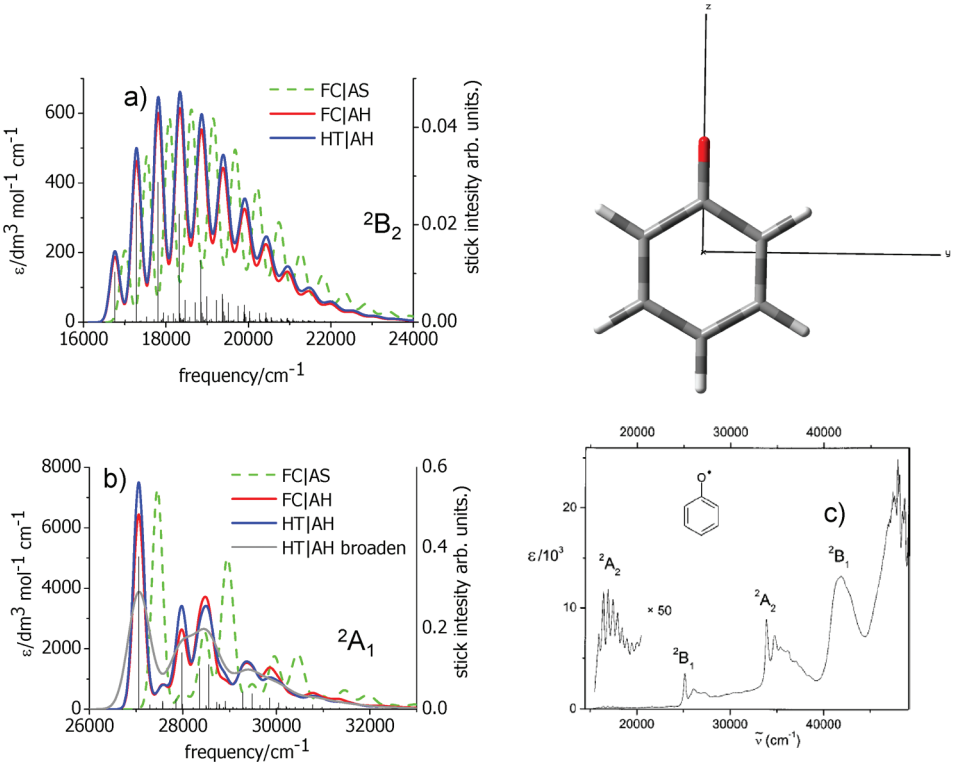

Figure 3. Absorption spectrum for the (a) $D_0 \rightarrow D_2$ (labeled $^2A_2$ in panel c) and (b) $D_0 \rightarrow D_3$ (labeled $^2B_1$ in panel c) transitions of phenoxyl radical, computed according to different models, convoluted with a Gaussian lineshape with HWHM = 0.033 eV. For $D_0 \rightarrow D_3$, a spectrum convoluted with a Gaussian lineshape with HWHM = 0.066 eV (labeled as "broaden" in the inset) also is reported. Stick spectra refer to the HT|AH calculation. (c) The experimental spectrum is also reported, for comparison (reprinted with permission from ref 59, Copyright 2001, American Institute of Physics).

dx.doi.org/10.1021/ct200054w |*J. Chem. Theory Comput.* 2011, 7, 1824–1839

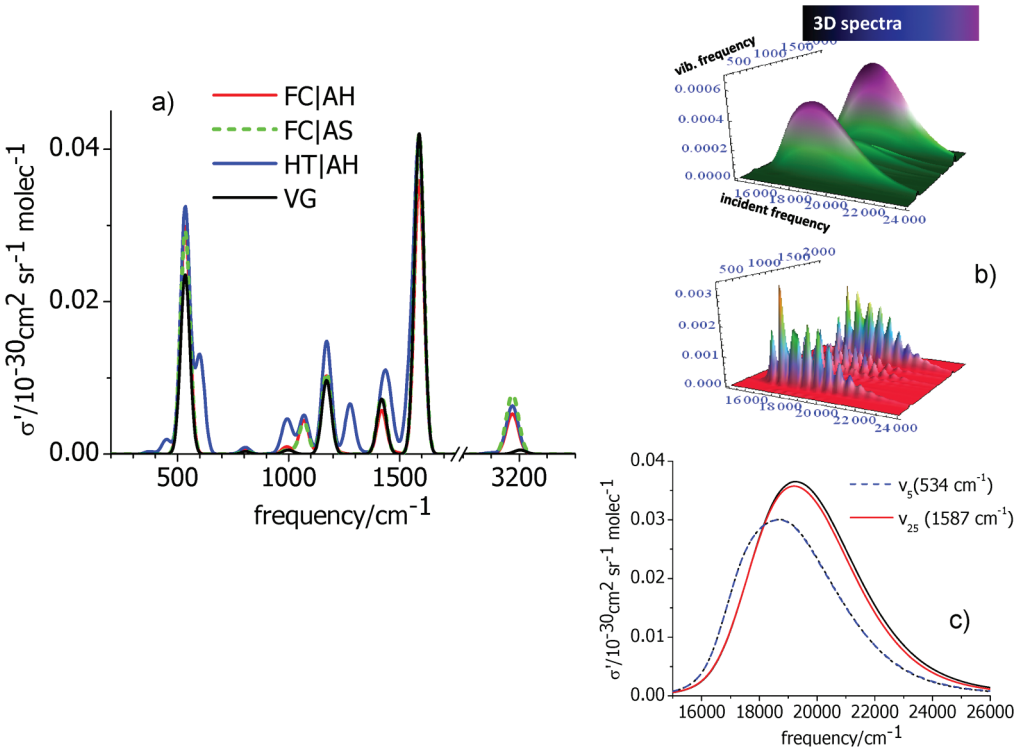

Figure 4. (a) Comparison of the RRS spectrum resonant with the maximum of the $D_0 \rightarrow D_2$ transition, computed according to different models ($\gamma = 0.1$ eV). (b) FC resonance Raman 2D spectrum for the $D_0 \rightarrow D_2$ transition for $\gamma = 0.1$ eV (upper panel) and 0.02 eV (lower panel). (c) FC Raman excitation profile resonant with the $D_0 \rightarrow D_2$ transition for two different vibrational modes for a $\gamma = 0.1$ eV. A convergence test is also shown in the case of $\nu_{25}^{(0)}$ (the accuracy parameter N^{max} is varied from 10^5 to 10^7, see red and black straight lines). The vibrational stick RRS bands have been convoluted with a Gaussian lineshape, with HWHM = 25 cm^{-1} (not normalized, i.e., its maximum is 1).

of the peak intensities, which are more pronounced for the D_3 state.

Overall, the reproduction of the experimental absorption spectrum (which was recorded in an argon matrix at a temperature of 7 K, see ref 59), shown in Figure 3c, is good, thus showing the reliability of the combination of TD-DFT with our approach to calculate vibronic progressions.

2. RR Scattering for the $D_0 \rightarrow D_2$ Transition: Fundamentals and Overtones. Moving to RRS, in Figure 4, the spectrum obtained for the $D_0 \rightarrow D_2$ transition is reported (Figure 4a) as a function of the level of description of the RR phenomenon. All the spectra have been computed assuming an excitation at the vertical transition energy and, if not differently stated, an excited-state lifetime of $\gamma = 0.1$ eV, apart from those computed according to the gradient approximation, which are not explicitly dependent on these parameters and are thus given in arbitrary units. Note that, in the present manuscript, γ is used as a purely phenomenological parameter: the dependence of the description of RR spectra and Raman excitation profiles on γ will be underlined for selected cases (*vide infra*). Calculated vertical transition energies (and not estimated experimental ones) have been used (see Figure 2 for their values). Note further that, here and afterward, in order to be free of possible anharmonic effects that would complicate the comparison of the different harmonic models, the excited-state energy gradient values are actually retrieved, by invoking the harmonic approximation, from the displacements of the equilibrium structures, according to the relations given in eq 29.

The convergence of the reported spectra is very good. As shown in the Supporting Information, spectra evaluated with $N^{max} = 10^5$ are exactly superimposable to the more accurate ones computed with $N^{max} = 10^7$, even if, in the first case, a maximum error of 7% still remains, as far as the convergence to the analytical sums for fundamentals is concerned.

A general overview of the spectra reported in Figure 4 indicates remarkable differences in the predictions obtained by the different models all over the spectrum, and that mostly involve vibrations in the 400−700 cm^{-1} and 1000−1500 ranges (out-of-plane and in-plane ring bending and C−O stretching modes). By analyzing the spectra in more detail, two dominant lines can be seen at the FC level, corresponding to the fundamentals of the $\nu_5^{(0)}$ and $\nu_{25}^{(0)}$ modes (a combination of ring CC stretchings). It is remarkable that these lines are strictly correlated to the progressions observed in the absorption spectrum, but also that, at the same time, noticeable differences arise. In fact, the $\nu_5^{(0)}$ mode gives rise to the main progression in the absorption spectrum, and the progressions at ∼1550−1600 cm^{-1} (although more than one mode is involved, because of Duschinsky effects) are mainly correlated with a remarkable displacement along the $\nu_{25}^{(0)}$ mode. Nonetheless, while the progression along the $\nu_5^{(0)}$ mode is, by far, the dominant one in the absorption spectrum, the RRS intensity along this mode is overcome by that along the $\nu_{25}^{(0)}$ mode. Moreover, the difference between the various computational approaches is more evident in the RRS spectrum than in the absorption spectrum. In particular, the introduction of HT effects causes a markedly different intensity pattern, leading to the appearance of new bands that are not predicted by the other models. This is the case, for example, of the bands at 600 cm^{-1} and 1276 cm^{-1}, which are respectively assigned to the fundamentals of the $\nu_6^{(0)}$ and $\nu_{19}^{(0)}$ modes, which, in fact, exhibit large

derivatives of the transition dipole moment $\vec{\mu}^{02}$. Despite this fact, these two modes (or, better, the corresponding D_2 modes) do not appear to give appreciable signatures in the absorption spectrum.

It is also worth highlighting some marked differences between the VG and FC|AS spectra. In fact, while, for small displacements, the two models are expected to give similar results, differences arise when the displacements are relevant. The two peaks at 1068 and 3175 cm^{-1} are overtones (2 quanta) of the dominant fundamental bands along the $\nu_5^{(0)}$ and $\nu_{25}^{(0)}$ modes, which have remarkable intensity but are not described within the gradient approach (at least in its standard implementation). Finally, the differences among the FC|AS and FC|AH models are only marginal (see, for example, the overtone band at 3175 cm^{-1}), thus indicating that Duschinsky effects play only a minor role in the present case.

2D RRS Spectra and Raman Excitation Profiles. Figure 4b reports the RRS 2D spectrum as a function of the incident frequency and the difference between the frequencies of the incident and scattered light (indicated as vibrational frequency, i.e., the same coordinate already adopted in Figure 4a). Because of some arbitrariness in the choice of the γ parameter, two possibilities are compared, corresponding to a short lifetime (γ = 0.1 eV) and a long lifetime (γ = 0.01 eV). As expected, the 2D spectra appear very different for the two values of γ and are much more resolved for a long lifetime. A more-detailed analysis is possible by examining cuts of the 2D spectra obtained by fixing the vibrational frequency (i.e., the so-called Raman excitation profiles). Figure 4c reports such spectra for the two dominant bands: the fundamentals of the $\nu_5^{(0)}$ and $\nu_{25}^{(0)}$ modes. For the $\nu_{25}^{(0)}$ mode, the results of two different calculations are reported, performed with $N^{max} = 10^5$ and $N^{max} = 10^7$ (black and red straight lines), to show that the method permits to reach a very good convergence, even with respect to the excitation profile. Focusing on the interpretative aspects, it is worth noting that the relative RR intensities of the two modes are dependent on the frequency of the exciting light, and, in particular, because of the shape of the curves, the band at 534 cm^{-1} may or may not overtake that at 1587 cm^{-1}, depending on the exciting radiation.

At this point of the discussion, a general comment is appropriate. Given the current state of the art, the γ value is not easily computable *ab initio*, so it is commonly treated as a phenomenological parameter. Moreover, the computational prediction of the absolute position of the excited states is always affected by some error, so it may not be easy to establish a one-to-one correspondence between the experimental incident frequency and the vertical frequency at which the RRS spectrum is simulated. Therefore, it is very encouraging that the method presented here can efficiently compute spectra, as a function of these parameters. In fact, this may allow for a careful check of the sensitivity of the predictions on these parameters, in order to provide a robust interpretation, which is possibly not biased by particular and possibly unappropriate choices of such values.

3. RR Scattering for the $D_0 \rightarrow D_3$ Transition: Fundamentals and Overtones. Figure 5 shows calculated RRS spectra of the $D_0 \rightarrow D_3$ transition, as a function of the choice of the computational model. Similar to that observed for the $D_0 \rightarrow D_2$ transition, in this case, the predicted spectral shape also changes remarkably as the computational model varies with the appearance/disappearance of some peaks, the most evident differences being those introduced by HT effects (the HT|AH model). Comparison with the experiment (taken from ref 60) documents a good overall

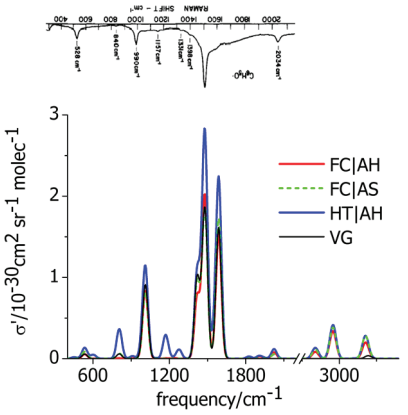

Figure 5. RRS spectrum resonant with the maximum of the $D_0 \rightarrow D_3$ transition, computed according to different models. VG calculation only includes fundamental transitions and is reported in arbitrary units. The experimental spectrum is reported for comparison (reprinted with permission from ref 60, Copyright 1984, American Institute of Physics). Vibrational stick RRS bands have been convoluted with a Gaussian lineshape, with HWHM = 25 cm^{-1} (not normalized, i.e., its maximum is 1).

agreement, especially if the low resolution of the experimental data is considered. In more detail, our calculation correctly predicts the dominant band to be observed at ~1500 cm^{-1} (assigned to the fundamental of the $\nu_{23}^{(0)}$ mode with a frequency of 1478 cm^{-1}), and that such a band is accompanied by a second blue-shifted peak, assigned to the $\nu_{25}^{(0)}$ mode at a frequency of 1587 cm^{-1}, whose intensity, however, is significantly overestimated in our calculations when compared with the experiment, where it simply appears as a shoulder. The positions of minor peaks at ~1200, 1000, 800, and 600 cm^{-1} are also nicely predicted, as well as, in most cases, the relative order of their intensities. The strongest band at 1011 cm^{-1} is assigned to the fundamental of the $\nu_{15}^{(0)}$ mode. Note that, similar to that observed in the $D_0 \rightarrow D_2$ spectrum, in the region above 3000 cm^{-1}, some small but non-negligible peaks arise. These latter might be erroneously assigned to CH stretchings, whereas they are actually due to overtones of the fundamental bands in the 1500 cm^{-1} region. This can be easily recognized by noticing that they are absent in VG calculations, which only account for fundamentals.

Raman Excitation Profiles. In Figure 6, Raman excitation profiles resonant with the $D_0 \rightarrow D_3$ transition are reported for two selected normal modes. FC|AH and HT|AH results are compared in Figure 6a, where absorption spectra, obtained using the same broadening (0.1 eV), also are given, for comparison. The difference between FC and HT is not relevant for the band at 1011 cm^{-1} (only a shift in the intensity), whereas the difference is more substantial for the mode at 1478 cm^{-1}. Both FC and HT models, however, predict a larger RR intensity for this last band. Figure 6b only reports FC results, computed with a much narrower linewidth (γ = 0.02 eV), documenting that the shape of the profile is hugely dependent on the chosen linewidth, and that, for small values, the relative intensity of the two peaks may become drastically dependent on the incident frequency. Specifically, while the intensity of the 1011 cm^{-1} peak is higher than that of the 1478 $^{-1}$ one when the exciting frequency is in resonance with the 0−0 transition at ~27 000 cm^{-1}, in two different regions—namely, at ~28 800 and 30 000 cm^{-1}—the 1011 cm^{-1} peak is almost completely quenched and it is overcome by the 1478 cm^{-1} peak, by more than 1 order of magnitude.

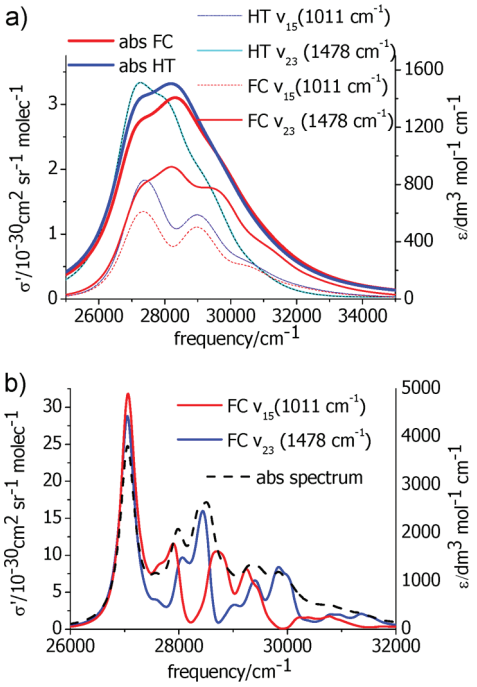

Figure 6. (a) FC and HT Raman excitation profiles resonant with the $D_0 \rightarrow D_3$ transition for two different vibrational modes and for γ = 0.1 eV. For HT computations, a convergence test also is reported by giving the results obtained by setting the accuracy parameter as N^{max} = 10^6 and 10^7. RR profiles are compared with the corresponding absorption spectra computed with a Lorentzian broadening, with the same linewidth and γ = 0.1 eV. (b) FC Raman excitation profile resonant with the $D_0 \rightarrow D_3$ transition for two different vibrational modes and a small linewidth and γ = 0.02 eV (solid lines). The RR profiles are compared with the corresponding absorption spectrum, computed with the same Lorentzian broadening.

4. RR Scattering for the $D_0 \rightarrow D_3$ Transition: Combination Bands. The unusually high-frequency experimental peak at 2034 cm^{-1} (see Figure 5) is not reproduced in our calculations, which do predict a band in that region (2022 cm^{-1}), assigned to the first overtone of $\nu_{15}^{(0)}$, but its intensity is much smaller than its experimental counterpart. Based on the position of the strongest experimental band slightly above 1500 cm^{-1} and the secondary band at 528 cm^{-1}, it may be suggested that the peak at 2034 cm^{-1} corresponds to a combination band of the two modes, giving rise to these fundamentals.

A brute-force SOS calculation of all of the possible combinations of two bands (435 pairs) would require a very expensive calculation. Analysis of the TT expression for combination bands in eq 26 indicates that, apart the frequency-dependent Φ factors, their RRS intensities are expected to be dependent on the product of the displacements along the two modes, in the same way as fundamentals and overtones are dependent on such displacements and their powers. Here, based on these considerations, we have selected the combination bands of pairs of modes corresponding to the eight most-intense fundamentals (namely, $\nu_5^{(0)}$, $\nu_{10}^{(0)}$, $\nu_{15}^{(0)}$, $\nu_{17}^{(0)}$, $\nu_{19}^{(0)}$, $\nu_{21}^{(0)}$, $\nu_{23}^{(0)}$, $\nu_{25}^{(0)}$). The RRS spectra obtained including either only fundamentals and overtones (up to the quantum number n = 3) for each mode or also the two-mode combination bands (quantum numbers 1 + 1) of the eight selected modes are compared in Figure 7. Here, for an easier individuation, the fundamentals and overtones of mode n with quantum number q are labeled as n^q and the combination bands

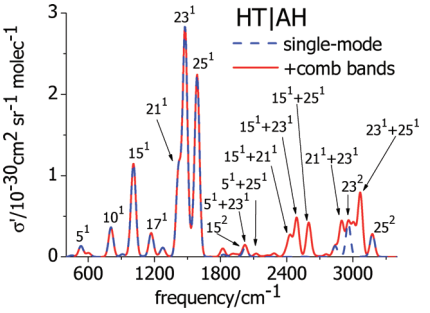

Figure 7. RRS spectrum resonant with the maximum of the $D_0 \rightarrow D_3$ transition, computed according to the HT|AH model, including only fundamentals and overtones (blue dashed line, the same data reported in blue in Figure 5, here denoted by the label "single-mode") or also the main combination bands of two modes (red solid line). The vibrational stick RRS bands have been convoluted with a Gaussian, with HWHM = 25 cm^{-1} (not normalized, i.e., its maximum is 1).

of modes n and m with quantum numbers q and r are labeled as $n^q + m^r$. It is interesting to note that combination bands strongly modify the spectral shape at ~2500 cm^{-1} and ~3000 cm^{-1}, creating new features in a region otherwise totally flat (~2500 cm^{-1}), or dominating the close-lying overtones of the modes involved in the combination (~3000 cm^{-1}). As an example, the combination band 23^1+25^1, of the $\nu_{23}^{(0)}$ and $\nu_{25}^{(0)}$ modes, is more intense than the overtone 25^2, even if the fundamental 23^1 is more intense than 25^1. In agreement with what we speculated at the beginning of this section, in the region of 2000−2100 cm^{-1}, two combination bands arise—$5^1 + 23^1$ and $5^1 + 25^1$ respectively—at frequencies of 2013 cm^{-1} (enforcing the 15^2 band at 2022 cm^{-1}) and 2122 cm^{-1}, but their intensities (relative to the spectrum maximum at ~1500 cm^{-1}) are underestimated, with respect to the experimental band at 2034 cm^{-1}; this feature was expected, since the computed fundamental 5^1 is actually sensibly weaker than the experimental band at 528 cm^{-1}. As a last remark, it is interesting to note that the band $5^1 + 25^1$ is ~25% higher than $5^1 + 23^1$, even if the fundamental 23^1 is more intense than 25^1, showing that the exact intensities of combination bands cannot be trivially deduced from the intensities of the fundamentals of the involved modes.

B. IDMN in Acetonitrile and Cyclohexane Solutions. In this section, we present results for IDMN in a cyclohexane and acetonitrile solution. IDMN has 96 normal modes and, therefore, is a much larger system than that of a phenoxyl radical (30 normal modes). Based on the results of a previous study performed in ref 52 on IDMN RRS spectra in solution, calculations were performed by adopting CAMB3LYP and the 6-311G(d,p) basis sets. In the Supporting Information, we checked that the dependence of the computed spectra on the basis set is very weak, using calculations with the smaller 6-31G(d) basis set.

1. Absorption Spectra. Figure 8 sketches the calculated absorption spectra in the two solvents, according to different computational models. In this case, only the first singlet excited state is relevant to the spectrum. Apart from a general blue-shift in all the spectrum, because of the particular choice of the combination of DFT functional and basis set, the comparison between calculations and experimental findings, given in Figure 8b and taken from ref 61, shows generally good agreement. In both solvents, the relative intensity of the bluemost peak appears slightly too small, thus indicating a slight underestimation of geometry displacements or Duschinsky mixings.

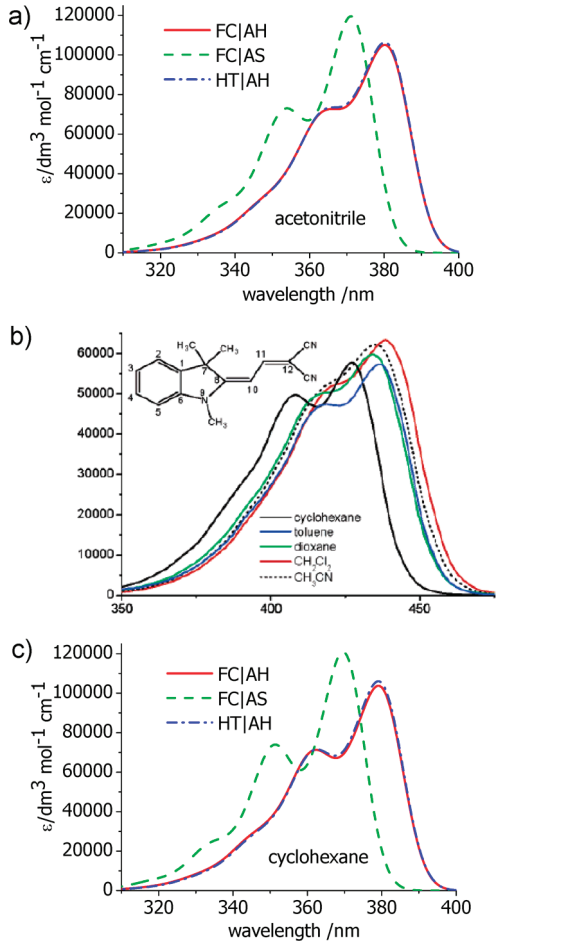

Figure 8. Calculated absorption spectrum of IDMN in (a) acetonitrile and (c) cyclohexane, computed according to different models and convoluted with a Gaussian lineshape, with HWHM = 0.05 eV. (b) For comparison, the experimental spectrum taken from ref 61 also is reported.

Inhomogeneous broadening is larger in acetonitrile than in cyclohexane, because of their different polarities. This is the main reason why, in the experimental spectrum, the two peaks almost coalesce in acetonitrile while they are better distinguished in cyclohexane. *A priori* estimate of the electrostatic contribution to the broadening is becoming feasible and is the subject of work we currently have in progress, while the treatment of the nonelectrostatic (dispersion, repulsion, and cavitation) contributions might be addressed by a recent approach presented in the literature.[62] At the state of the art, the broadening is usually treated as a phenomenological parameter; therefore, for the scope of the present article, we decided to avoid a proliferation of parameters, convoluting the stick spectra in the two solvents by the same Gaussian lineshape (fwhm = 0.1 eV). Nonetheless, the two peaks in acetonitrile still appear to coalesce slightly more than those in cyclohexane, highlighting an interesting pure vibronic contribution to broadening, even if it is clearly of secondary importance, with respect to the effect of solvent fluctuations.

The inclusion of HT terms causes only negligible effects, whereas more-substantial differences are observed by varying the model to approximate the excited state PES (compare the AS and AH results). In both solvents, the AH results, which include the

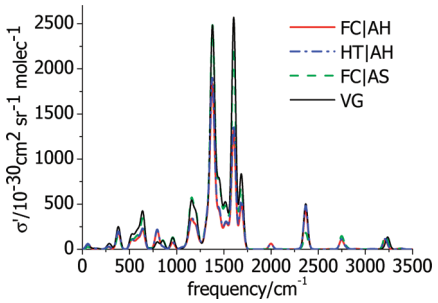

Figure 9. Calculated RRS spectrum of IDMN in acetonitrile excited at the band maximum, assuming γ = 0.1 eV, and obtained by exploiting different computational models. The vibrational stick RRS bands have been convoluted with a Gaussian lineshape, with HWHM = 25 cm^{-1} (not normalized, i.e., its maximum is 1).

effect of frequency changes and Duschinky mixings, outperform the AS results, as far as the ratio of the intensity of the peaks is concerned.

2. Resonance Raman Scattering. The calculated RRS spectrum of IDMN in acetonitrile is reported in Figure 9, as a function of the different models used to treat the vibronic coupling. The spectrum obtained by exploiting the VG model is also shown. The vibrational modes giving rise to the most intense peaks involve the motion of the π-system (in the 1200−1700 cm^{-1} range) and the nitrile groups stretching (at ∼2350 cm^{-1}). As already seen for the absorption spectrum, HT effects on the transition dipoles are negligible for RRS, whereas changing the level of accuracy of the description of the PES of the resonant state has a remarkable impact on the relative intensities of the various peaks, which is clear via comparison of the AS and VG results with those provided by the full AH model. This highlights the possible importance of the effect of frequency changes and Duschinsky mixings in resonance Raman spectra. It is worthy to note, for example, that the relative intensities of the two major peaks at ∼1400 and 1600 cm^{-1} are remarkably dependent on the introduction of Duschinsky effects. Actually, these two peaks arise from fundamentals of the 62 and 77 modes, respectively, and these two modes are affected by strong Duschinsky mixings. In fact, respectively, 9 and 10 excited-state normal modes are needed to project them by more than 95%. Therefore, it is not surprising that, as shown in the Supporting Information, the calculation of overtones along these modes is more challenging for the computational method. Figure 10 compares the FC|AH RRS spectra in acetonitrile (Figure 10a) and cyclohexane (Figure 10c) with the experimental spectra (Figure 10b). Both theoretical stick spectra, and spectra obtained by their Gaussian convolution, with HWHM = 15 cm^{-1}, are given. All the most intense lines correspond to fundamental transitions and are labeled by the number (in order of increasing frequency) of the involved normal mode. Overall, the theoretical results are in very good agreement with their experimental counterparts and nicely reproduce the main structure characterized by three multiplets lying at ∼1150, ∼ 1350 and ∼1550 cm^{-1}, both in terms of their positions (apart from a slight blueshift, expected since no scaling factor has been applied on the frequencies), and in terms of their relative intensities. Also, the agreement in the relative intensities is satisfactory. Focusing on the results in acetonitrile, comparison of the relative heights of the FC|AH multiplets at ∼1350 and ∼1550 cm^{-1} with those predicted by the simpler FC|AS and VG models indicates that the inclusion of

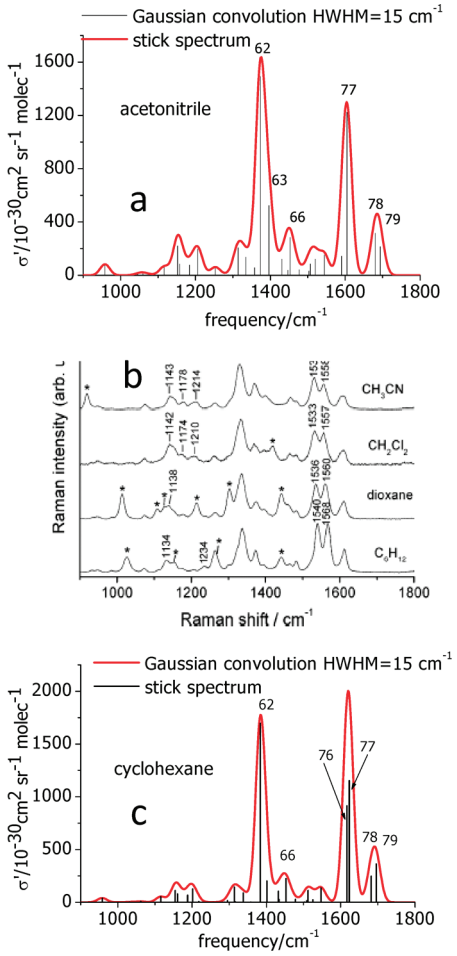

Figure 10. Stick and Gaussian convoluted (HWHM =15 cm^{-1}) RRS spectra of IDMN in (a) acetonitrile and (c) cyclohexane, computed according to the FC|AH model for an excitation at the band maximum. (b) Experimental RR spectrum for an excitation at 391 nm, taken from ref 61.

Duschinsky effects and frequency changes significantly improves the agreement with the experiment (see Figure 10).

As far as the solvent effect is concerned, comparison of the theoretical and experimental spectra shows that the combination of the PCM with our approach is able to account for the peculiarities in the spectrum introduced by the nature of the medium. In particular, the presence of the solvent and its polarity characteristics do not simply cause a shift in the bands and/or an homogeneous increase/decrease of band intensities, but the relative intensities of the peaks remarkably change, as a result of the nature of the solute−solvent interactions, thus causing an overall different intensity pattern in the spectrum. Major differences in the computed spectra in the two solvents arise in the relative heights of the multiplet at ∼1350 and ∼1550 cm^{-1} (the blue one is enhanced in cyclohexane, in very good agreement with the experimental findings). Also, the inner structure of each multiplets can be analyzed. While the two-peak structure of the multiplet at ∼1350 cm^{-1} is perfectly reproduced in our calculations, the three-peak structure of the bluemost multiplet is apparently not reproduced in the convoluted spectrum, where only two peaks appear (with the middle peak being apparently missing). Nonetheless, analysis of the stick spectra shows that two different transitions contribute to the major peak at ∼1600 cm^{-1}, in agreement with the experiment, but they are too close to each other, so they coalesce in a single peak after convolution. Finally, the experimental multiplet at ∼1150 cm^{-1} shows a richer and more asymmetric structure in acetonitrile than in cyclohexane; even this feature is nicely reproduced by our calculations.

It is also worth noting that computed spectra in Figures 9 and 10 assume an excitation at the vertical transition, while experimental spectra were recorded at 391 nm, which is an excitation blue-shifted by more than 2000 cm^{-1}, with respect to the band maximum (estimated for an infinite broadening) both in acetonitrile and cyclohexane. By taking into account such a blue-shift, the computed RRS spectra change only slightly for the chosen γ value (see the Supporting Information).

To end this section, it is worth noting that the noticeable improvement of the use of our full FC|AH model, with respect to other methodologies, is further evidenced in comparison with previous calculated spectra reported in the literature.[52]

V. SUMMARY, CONCLUSIONS, AND PERSPECTIVES

We have presented a time-independent method, grounded in the harmonic approximation, and based on a sum-over-states (SOS) calculation of the polarizability tensor that provides several improvements, with respect to the commonly adopted models for the computation of vibrational resonance Raman scattering (RRS) spectra. In particular, our method is able to include Duschinsky and Herzberg−Teller (HT) effects, and to consider not only fundamental transitions but also overtones and combination bands. In addition, its computational effectiveness allows one to compute two-dimensional (2D) RRS spectra, as a function of both the incident and the scattered frequencies, and to explore the dependence of the spectra on the excited-state lifetime, which is a parameter that is usually treated phenomenologically. Moreover, the present method paves the way for analysis of the interferential features that occur when more than one excited state is in quasi-resonance with the excitation frequency. Beyond that, it is worthwhile to note that the approach presented here can be extended rather straightforwardly to the description of other spectroscopic phenomena related to RRS, such as resonance Raman optical activity or resonance hyper-Raman, by also including, for these spectroscopies, Duschinsky and HT effects.

The computational burden of RRS calculations increases significantly with respect to absorption spectra. In this respect, the numerical evidence that the convergence of RRS spectra does not require the full convergence to the analytical sums (either the RRS ones or the absorption ones) is very encouraging, because it allows one to strongly decrease the computational cost. Nonetheless, although, in principle, the method also can be adopted for extensive exploration of the intensities of combination bands involving two or more modes, computational efficiency would probably require refinement and further optimization of the selection schemes. In this respect, in future work, we plan to explore different computational strategies, based on the time-dependent formalism introduced by Heller and collaborators.[6,7]

■ ASSOCIATED CONTENT

Supporting Information. Convergence tests of the results for the phenoxyl radical in the gas phase and for FC|AH spectra of IDMN in acetonitrile; FC|AH RRS spectra and RR excitation profiles for IDMN in acetonitrile at different excitation

frequencies; comparison of the absorption and RRS spectra of IDMN computed with the 6-311G(d,p) and 6-31G(d) basis sets. (PDF) This material is available free of charge via the Internet at http://pubs.acs.org.

AUTHOR INFORMATION

Corresponding Author

*E-mail addresses: fabrizio.santoro@iccom.cnr.it (F.S.), chiara@dcci.unipi.it (C.C.).

ACKNOWLEDGMENT

The computational resources for this work have been provided through the CNR-Village Network (http://village.pi.iccom.cnr.it). F.S. acknowledges the support of Italian MIUR (PRIN 2008) and IIT (Project IIT-Seed "Helyos").

REFERENCES

(1) Long, D. A. *The Raman Effect*; Wiley: Chichester, U.K., 2002.

(2) Myers, A. B. Resonance Raman Intensities and Charge-Transfer Reorganization Energies. *Chem. Rev.* **1996**, *96*, 911.

(3) Barone, V.; Improta, R.; Rega, N. Quantum Mechanical Computations and Spectroscopy: From Small Rigid Molecules in the Gas Phase to Large Flexible Molecules in Solution. *Acc. Chem. Res.* **2008**, *41*, 605–616.

(4) Kelley, A. M. Resonance Raman and Resonance Hyper-Raman Intensities: Structure and Dynamics of Molecular Excited States in Solution. *J. Phys. Chem. A* **2008**, *112*, 11975.

(5) Peticolas, L.; Rush, T., III. Ab Initio Calculations of the Ultraviolet Resonance Raman Spectrum of Uracil. *J. Comput. Chem.* **1995**, *16*, 1261–1270.

(6) Heller, E. J.; Lee, S.-Y. Time Dependent Theory of Raman Scattering. *J. Chem. Phys.* **1979**, *71*, 4777–4788.

(7) Heller, E. J.; Sundberg, R. L.; Tannor, D. Simple aspects of Raman scattering. *J. Phys. Chem.* **1982**, *86*, 1822–1833.

(8) Kramers, K. A.; Heisenberg, W. Uber die Streuung von Strahlung durch Atome. *Z. Phys.* **1925**, *31*, 681.

(9) Dirac, P. A. M. The Quantum Theory of Dispersion. *Proc. R. Soc. London, Ser. A* **1927**, *114*, 710.

(10) Warshel, A.; Dauber, P. Calculations of Resonance Raman Spectra of Conjugated Molecules. *J. Chem. Phys.* **1977**, *66*, 5477–5488.

(11) Jensen, L.; Zhao, L. L.; Autschbach, J.; Schatz, G. C. Theory and method for calculating resonance Raman scattering from resonance polarizability derivatives. *J. Chem. Phys.* **2005**, *123*, 174110.

(12) Albrecht, A. C. On the Theory or Raman Intensities. *J. Chem. Phys.* **1961**, *34*, 1476.

(13) Blazej, D. C.; Peticolas, W. L. J. Ultraviolet resonance Raman excitation profiles of pyrimidine nucleotides. *J. Chem. Phys.* **1980**, *72*, 3134–3142.

(14) Zheng, R.-H.; Wei, W.-M. Density Functional Theory Study on Anti-resonance in Preresonance Raman Scattering for Naphthalene Molecules. *J. Phys. Chem. A* **2007**, *111*, 3652–3660.

(15) Kiewisch, J.; Neugebauer, K.; Reiher, M. Selective calculation of high-intensity vibrations in molecular resonance Raman spectra. *J. Chem. Phys.* **2008**, *129*, 204103.

(16) Kane, A. K.; Jensen, L. Calculation of Absolute Resonance Raman Intensities: Vibronic Theory vs Short-Time Approximation. *J. Phys. Chem. C* **2010**, *114*, 5540–5546.

(17) Jarzecki, A. A. Quantum-Mechanical Calculations of Resonance Raman Intensities: The Weighted-Gradient Approximation. *J. Phys. Chem. A* **2009**, *113*, 2926–2934.

(18) Luber, S.; Neugebauer, J.; Reiher, M. Enhancement and de-enhancement effects in vibrational resonance Raman optical activity. *J. Chem. Phys.* **2010**, *132*, 044113.

(19) Neugebauer, J.; Hess, B. A. Resonance Raman spectra of uracil based on Kramers−Kronig relations using time-dependent density functional calculations and multireference perturbation theory. *J. Chem. Phys.* **2004**, *120*, 11564.

(20) Neugebauer, J.; Baerends, E. J.; Efremov, E. V.; Ariese, F.; Gooijer, C. Combined Theoretical and Experimental Deep-UV Resonance Raman Studies of Substituted Pyrenes. *J. Phys. Chem. A* **2005**, *109*, 2100.

(21) Guthmuller, J.; Champagne, B. Resonance Raman Scattering of Rhodamine 6G as Calculated by Time-Dependent Density Functional Theory: Vibronic and Solvent Effects. *J. Phys. Chem. A* **2008**, *112*, 3215–3223.

(22) Jensen, L.; Schatz, G. C. Resonance Raman Scattering of Rhodamine 6G as Calculated Using Time-Dependent Density Functional Theory. *J. Phys. Chem. A* **2006**, *110*, 5973–5977.

(23) Guthmuller, J.; Champagne, B. Time dependent density functional theory investigation of the resonance Raman properties of the julolidinemalononitrile push-pull chromophore in various solvents. *J. Chem. Phys.* **2007**, *127*, 164507.

(24) Guthmuller, J.; Champagne, B.; Moucheron, C.; Kirsch-De Mesmaeker, A. Investigation of the Resonance Raman Spectra and Excitation Profiles of a Monometallic Ruthenium(II) $[Ru(bpy)_2(HAT)]^{2+}$ Complex by Time-Dependent Density Functional Theory. *J. Phys. Chem. B* **2010**, *114*, 511–520.

(25) Herrmann, C.; Neugebauer, J.; Presselt, M.; Uhlemann, U.; Schmitt, M.; Rau, S.; Popp, J.; Reiher, M. The First Photoexcitation Step of Ruthenium-Based Models for Artificial Photosynthesis Highlighted by Resonance Raman Spectroscopy. *J. Phys. Chem. B* **2007**, *111*, 6078–6087.

(26) Hizhnyakov, V.; Tehver, I. Transform Method in Resonance Raman Scattering with quadratic Franck-Condon and Herzberg-Teller Interactions. *J. Raman Spectrosc.* **1988**, *19*, 383–388.

(27) Chan, C. K.; B., P. J. Temperature Effects in the time correlator theory of Resonance Raman Scattering. *J. Chem. Phys.* **1983**, *79*, 5234.

(28) Tonks, D. L.; B., P. J. Diagrammatic Theory of temperature-dependent resonance Raman scattering from polyatomic systems with general harmonic potential surfaces. *J. Chem. Phys.* **1988**, *88*, 738.

(29) Lu, H. M.; Page, J. B. General transform technique including mode mixing and non-Condon coupling in resonance Raman scattering. *J. Chem. Phys.* **1990**, *90*, 5315.

(30) Priyutov, M. V.; Burova, T. G. *Opt. Spectrosc. (USSR)* **1988**, *64*, 108.

(31) Priyutov, M. V.; Burova, T. G. *Opt. Spectrosc. (USSR)* **1991**, *71*, 37.

(32) Sharp, T. E.; Rosenstock, H. M. Franck−Condon Factors for Polyatomic Molecules. *J. Chem. Phys.* **1963**, *41*, 3453–3463.

(33) Kupka, H.; Cribb, P. H. Multidimensional Franck−Condon integrals and Duschinsky mixing effects. *J. Chem. Phys.* **1986**, *85*, 1303.

(34) Ruhoff, P. T. Recursion relations for multi-dimensional Franck−Condon overlap integrals. *Chem. Phys.* **1994**, *186*, 355–374.

(35) Doktorov, E. V.; Malkin, I. A.; Man'ko, V. I. Dynamical symmetry of vibronic transitions in polyatomic molecules and the Franck−Condon principle. *J. Mol. Spectrosc.* **1977**, *64*, 302–326.

(36) Doktorov, E. V.; Malkin, I. A.; Man'ko, V. I. Dynamical symmetry of vibronic transitions in polyatomic molecules and the Franck−Condon principle. *J. Mol. Spectrosc.* **1975**, *56*, 1–20.

(37) Biczysko, M.; Bloino, J.; Santoro, F.; Barone, V. In *Computational Strategies for Spectroscopy: From Small Molecules to Nano Systems*; Barone, V., Ed.; Wiley: Chichester, U.K., 2011; pp 300−386.

(38) Hazra, A.; Nooijen, M. Derivation and efficient implementation of a recursion formula to calculate harmonic Franck−Condon factors for polyatomic molecules. *Int. J. Quantum Chem.* **2003**, *95*, 643–657.

(39) Dierksen, M.; Grimme, S. An efficient approach for the calculation of Franck−Condon integrals of large molecules. *J. Chem. Phys.* **2005**, *122*, 244101/1–9.

(40) Dierksen, M.; Grimme, S. The Vibronic Structure of Electronic Absorption Spectra of Large Molecules: A Time-Dependent Density Functional Study on the Influence of "Exact" Hartree−Fock Exchange. *J. Phys. Chem. A* **2004**, *108*, 10225–10237.

(41) Jankowiak, H.-C.; Stuber, J. L.; Berger, R. Vibronic transitions in large molecular systems: Rigorous prescreening conditions for Franck−Condon factors. *J. Chem. Phys.* **2007**, *127*, 234101/1–23.

(42) Santoro, F.; Improta, R.; Lami, A.; Bloino, J.; Barone, V. Effective method to compute Franck−Condon integrals for optical spectra of large molecules in solution. *J. Chem. Phys.* **2007**, *126*, 084509/1–13.

(43) Santoro, F.; Lami, A.; Improta, R.; Barone, V. Effective method to compute vibrationally resolved optical spectra of large molecules at finite temperature in the gas phase and in solution. *J. Chem. Phys.* **2007**, *126*, 184102/1–11.

(44) Santoro, F.; Lami, A.; Improta, R.; Bloino, J.; Barone, V. Effective method for the computation of optical spectra of large molecules at finite temperature including the Duschinsky and HerzbergTeller effect: The Qx band of porphyrin as a case study. *J. Chem. Phys.* **2008**, *128*, 224311/1–17.

(45) Santoro, F.; Barone, V. Computational approach to the study of the lineshape of absorption and electronic circular dichroism spectra. *Int. J. Quantum Chem.* **2010**, *110*, 476–486.

(46) Lin, N.; Santoro, F.; Luo, Y.; Zhao, X.; Barone, V. Theory for Vibrationally Resolved Two-Photon Circular Dichroism Spectra. Application to (R)-(+)-3-Methylcyclopentanone. *J. Phys. Chem. A* **2002**, *113*, 4198–4207.

(47) Barone, V.; Bloino, J.; Biczysko, M.; Santoro, F. Fully Integrated Approach to Compute Vibrationally Resolved Optical Spectra: From Small Molecules to Macrosystems. *J. Chem. Theory Comput.* **2009**, *5*, 540–554.

(48) Bloino, J.; Biczysko, M.; Santoro, F.; Barone, V. General Approach to Compute Vibrationally Resolved One-Photon Electronic Spectra. *J. Chem. Theory Comput.* **2010**, *6*, 1256.

(49) Frisch, M. J.; Trucks, G. W.; Schlegel, H. B.; Scuseria, G. E.; Robb, M. A.; Cheeseman, J. R.; Scalmani, G.; Barone, V.; Mennucci, B.; Petersson, G. A.; Nakatsuji, H.; Caricato, M.; Li, X.; Hratchian, H. P.; Izmaylov, A. F.; Bloino, J.; Zheng, G.; Sonnenberg, J. L.; Hada, M.; Ehara, M.; Toyota, K.; Fukuda, R.; Hasegawa, J.; Ishida, M.; Nakajima, T.; Honda, Y.; Kitao, O.; Nakai, H.; Vreven, T.; Montgomery, Jr., J. A.; Peralta, J. E.; Ogliaro, F.; Bearpark, M.; Heyd, J. J.; Brothers, E.; Kudin, K. N.; Staroverov, V. N.; Kobayashi, R.; Normand, J.; Raghavachari, K.; Rendell, A.; Burant, J. C.; Iyengar, S. S.; Tomasi, J.; Cossi, M.; Rega, N.; Millam, N. J.; Klene, M.; Knox, J. E.; Cross, J. B.; Bakken, V.; Adamo, C.; Jaramillo, J.; Gomperts, R.; Stratmann, R. E.; Yazyev, O.; Austin, A. J.; Cammi, R.; Pomelli, C.; Ochterski, J. W.; Martin, R. L.; Morokuma, K.; Zakrzewski, V. G.; Voth, G. A.; Salvador, P.; Dannenberg, J. J.; Dapprich, S.; Daniels, A. D.; Farkas, Ö.; Foresman, J. B.; Ortiz, J. V.; Cioslowski, J.; Fox, D. J. Gaussian 09, Revision A.02. Gaussian, Inc., Wallingford, CT, 2009.

(50) Guthmuller, J.; Champagne, B. Time dependent density functional theory investigation of the resonance Raman properties of the julolidinemalononitrile push-pull chromophore in various solvents. *J. Chem. Phys.* **2007**, *127*, 164507.

(51) Mennucci, B.; Cappelli, C.; Cammi, R.; Tomasi, J. A quantum mechanical polarizable continuum model for the calculation of resonance Raman spectra in condensed phase. *Theor. Chem. Acc.* **2007**, *117*, 1029.

(52) Mennucci, B.; Cappelli, C.; Guido, C. A.; Cammi, R.; Tomasi, J. Structures and Properties of Electronically Excited Chromophores in Solution from the Polarizable Continuum Model Coupled to the Time-Dependent Density Functional Theory. *J. Phys. Chem. A* **2009**, *113*, 3009.

(53) Miertus, S.; Scrocco, E.; Tomasi, J. Electrostatic interaction of a solute with a continuum. A direct utilization of ab initio molecular potentials for the prevision of solvent effects. *Chem. Phys.* **1981**, *55*, 117–129.

(54) Tomasi, J.; Mennucci, B.; Cammi, R. Quantum Mechanical Continuum Solvation Models. *Chem. Rev.* **2005**, *105*, 2999–3093.

(55) Califano, S. *Vibrational States*; Wiley, London, 1976.

(56) Duschinsky, F. *Acta Physicochim. URSS* **1937**, *7*, 551.

(57) Peluso, A.; Santoro, F.; Del Re, G. Vibronic coupling in electronic transitions with significant Duschinsky effect. *Int. J. Quantum Chem.* **1997**, *63*, 233.

(58) Santoro, F. *FCclasses: A Fortran 77 Code*; 2008. (Available via the Internet at http://village.pi.iccom.cnr.it; last accessed March 23, 2011.)

(59) Radziszewski, J. G.; Gil, M.; Gorski, A.; Spanget-Larsen, J.; Waluk, J.; Mróz, B. J. Electronic states of the phenoxyl radical. *J. Chem. Phys.* **2001**, *115*, 9733.

(60) Tripathi, G. N. R.; Schuler, R. H. Electronic states of the phenoxyl radical. *J. Chem. Phys.* **1984**, *81*, 113.

(61) Leng, W.; Wurthner, F.; Kelley, A. M. Solvent-Dependent Vibrational Frequencies and Reorganization Energies of Two Merocyanine Chromophores. *J. Phys. Chem. A* **2005**, *109*, 1570.

(62) Weijo, V.; Mennucci, B.; Frediani, L. Toward a General Formulation of Dispersion Effects for Solvation Continuum Models. *J. Chem. Theory Comput.* **2010**, *6*, 3358.